Electronic Supplementary Material (ESI) for Materials Horizons

Supporting Information File

Topotactic reduction of oxide nanomaterials: unique structure and electronic properties of reduced TiO_2 nanoparticles

Satoshi Tominaka,*[a,b] Hideki Yoshikawa,[c] Yoshitaka Matsushita,[d] and Anthony K. Cheetham*[b]

[a]International Center for Materials Nanoarchitectonics (WPI-MANA), National Institute for Materials Science (NIMS), Namiki 1-1, Tsukuba, Ibaraki 305-0044, Japan. Email: TOMINAKA.Satoshi@nims.go.jp

[b]Department of Materials Science and Metallurgy, University of Cambridge, Pembroke Street, Cambridge CB2 3QZ, UK. Email: akc30@cam.ac.uk

[c]Surface Chemical Analysis Group, Nano Characterization Unit, Advanced Key Technologies Division, NIMS, Sengen 1-2-1, Tsukuba, Ibaraki 305-0047, Japan.

[d]Materials Analysis Station, NIMS, Sengen 1-2-1, Tsukuba, Ibaraki 305-0047, Japan.

Contents

S1. Experimental details

Materials. "TiO_x-NP" was synthesized by reducing rutile TiO_2 nanoparticles (Ltd., TTO-51(N), 10-30 nm in diameter; Ishihara Sangyo Kaisha) with CaH_2 (≥ 90%, Aldrich) as reported previously.[1] "TiO_x-SC" was synthesized by reducing mirror-polished, (100)-oriented rutile TiO_2 single crystals (Furuuchi Chemical) as reported previously.[2] Before the reduction treatment, as-purchased mirror-polished, 0.5 mm thick single crystals were coated with a polymer film, cut into 5 mm × 5 mm pieces using a DISCO DAD3220 dicing saw (Tokyo, Japan), and then cleaned by rinsing with acetone and oxygen plasma treatment. The clean crystal was annealed in air at 1000 °C to decrease defects. The reduced products were cleaned with 0.1 M NH_4Cl/CH_3OH and distilled water. "Ti_2O_3" was purchased from Sigma-Aldrich (titanium(III) oxide, 99.9%). In addition, rutile TiO_2 nanoparticles and rutile TiO_2 nanorods (FTL-100, Ishihara Sangyo) were also reduced by $NaBH_4$ (Reagent Grade from Kanto Chemical) as reported previously.[3]

Pair distribution function analyses. The X-ray total scattering data were collected on a curved imaging plate using (*i*) Mo Kα ($\lambda = 0.7107$ Å) at 50 kV, 40 mA for 22 h (RINT RAPID-S, Rigaku) with a 0.3 mmφ collimator, and (*ii*) synchrotron X-ray ($\lambda = 0.65298$ Å) at BL15XU SPring-8. The synchrotron X-ray is perfectly polarized with a perpendicular-to-parallel ratio of 0.001. The laboratory instrument has a larger detection angle (>150°), which results in high-resolution pair distribution functions ($2\pi/Q_{max}$).

The total scattering data were treated using the PDFgetX2 program,[4] through the background subtraction, the X-ray polarization correction, the self-absorption correction and the Compton scattering correction. The corrected total structure functions ($Q_{max} = 17.0$ Å^{-1} for Mo Kα, $Q_{max} = 13.1$ Å^{-1} for synchrotron X-ray) were converted into PDFs by Fourier transform. The PDFs were analyzed by curve fitting using PDFgui,[5] in the interatomic distance up to 30 Å with a spherical particle model.[6]

Rietveld refinements. The diffraction data were analyzed by the Rietveld refinements using the GSAS program[7] within the EXPGUI interface[8] with the Shifted Chebyschev background function and the Type 4 profile function. The high-resolution data collected using synchrotron X-ray ($\lambda = 0.65298$ Å) was used for TiO_x-NP, and the data collected using Mo *Kα* ($\lambda = 0.7093, 0.7136$ Å) were used for Ti_2O_3 and TiO_2. For the TiO_x-NP refinements, three different crystal models were tested: (1) corundum structure in space group $R\overline{3}c$, (2) ilmenite-type structure in $R\overline{3}$, where all the cation sites are occupied with Ti^{3+} ions, and (3) $LiNbO_3$-type structure in $R3c$, where all the cation sites are occupied with Ti^{3+} ions. For the Ti_2O_3 refinements, a model consisting of three crystal phases of corundum Ti_2O_3, γ-Ti_3O_5 and Ti_3O_5 was used.

HX-PES. The occupied states including valence band and core-level electrons were analyzed by hard X-ray photoelectron spectroscopy (HX-PES) using synchrotron X-ray at BL15XU SPring-8 at a beam energy of 5.95 keV. This can analyze elemental states underneath the surface native oxide. The detectable depths for both Ti 2*p* and O 1*s* were estimated as ~21 nm, which was three times as deep as the calculated inelastic mean free path of the photoelectrons.[9] The data were collected on a R4000 semi-spherical analyzer (VG Scienta, Tokyo, Japan) with the pass energy of 200 eV under vacuum ($<10^{-6}$ Pa). The Fermi level was calibrated using a polycrystalline Au standard sample. The X-ray beam intensity was adjusted to avoid peak shifts originating from charging. The spectra were corrected through the background subtraction with the Shirley method, the Savitzky-Golay smoothing process, and intensity normalization based on the peak areas of Ti 2*p*, O 1*s* or valence bands.

The compositions of TiO_x-NP, TiO_x-SC and Ti_2O_3 were determined from the integrated intensities of and the relative sensitive factor of Ti 2*p* and O 1*s* peaks. The sensitive factor was determined from the spectra of a (100)-oriented TiO_2 single crystal. The compositions of TiO_x-NP, TiO_x-SC and Ti_2O_3 are $Ti_{1.64}O_3$, $Ti_{2.03}O_3$ and $Ti_{2.02}O_3$, respectively.

EELS. The electron energy-loss spectra (EELS) were measured using a JEM-2100F transmission electron microscope (TEM) (JEOL, Tokyo, Japan) at 200 kV in the diffraction mode with a 1 mm aperture. For this measurement, the cross-sectional TEM samples were prepared through the focused-ion beam process and the micro-sampling process using an FB-2100 FIM system (Hitachi High-Technologies, Tokyo, Japan). The

EELS of TiO_x-SC and the TiO_2 single crystal were measured along the direction parallel to the *b*-axis of the unreacted TiO_2.

The energy-loss near-edge structures (ELNES) of Ti *L*-edge and O *K*-edge were analyzed via the model-based deconvolution processes using the EELSModel3.0 program.[10] In the model, a power law background and hydrogenic cross-sections of Ti *L*-edge and O K-edge were used. Then, the low-loss spectrum obtained at the same conditions was convoluted as the core-loss spectrum using the FFT function in order to simulate the influence of peak broadening and multiple scattering. The fitted plots were interpolated with a cubic spline approximation. The energy-scales were calibrated by setting the O *K*-edge peak of the unreacted TiO_2 region at 531.0 eV.[11]

Optical absorption. The optical absorption spectra were calculated on the basis of the Kubelka–Munk theory from diffuse reflectance spectra measured using a V-570 UV-vis-NIR spectrometer (JASCO, Tokyo, Japan) with an ISN-470 integrating sphere detector in the wavelength range from 2000 to 220 nm. The nanoparticles were diluted with dry KCl to be 1 wt%, while the Ti_2O_3 particles were used without this process. The optical constants of TiO_x-SC were measured by spectroscopic ellipsometry using M-2000U (J. A. Woollam Japan, Tokyo, Japan) at the incidence angle of 80° in the wavelength range from 250 to 1000 nm. Optical absorption coefficient, α, was calculated from the extinction coefficient, k.

Thermogravimetric analyses. The compositions were determined by thermogravimetric analyses scanned at 1 °C min^{-1} in 200 mL min^{-1} air flow (SII EXSTAR6000). The samples were dried under vacuum just before the measurement.

Scanning electron microscope observations. The nanoparticles samples were observed using a Hitachi S4800 scanning electron microscope at 10 kV. The nanoparticles were dispersed in pure water using ultrasonication, dried on a TEM grid, and then observed without any surface coating.

Conductivity measurements. The temperature dependence of the resistance was measured from 8 to 300 K at *ca.* 1.2×10^{-5} Pa using a four probe method (bias: ± 0.5 V) with a GRAIL 10-408040LV cryogenic electrical characteristic measurement system (Nagase Techno-Engineering, Tokyo, Japan) and a 4200-SCS semiconductor characterization system (Keithley Instruments, Tokyo, Japan).

The reduced single crystals were carefully cut into 2 mm × 5 mm pieces using a DISCO DAD3220 dicing saw (Tokyo, Japan) after protecting the surface with a polymer film. Then, four Au lines 100 μm wide (100 nm thick with a 10 nm Ti adhesion layer) were deposited by electron beam evaporation through a Si stencil mask. The width and length of the conduction pathway was defined by the mask.

The thickness of the reduced region was measured by cross-sectional transmission electron microscope (TEM) observation using a JEM-2100F microscope (JEOL, Tokyo Japan) at 200 kV. The cross-sectional TEM samples were prepared using the focused-ion beam and microsampling method on an FB-2100 FIB system (Hitachi High-Technologies, Tokyo, Japan).

S2. X-ray total scattering data

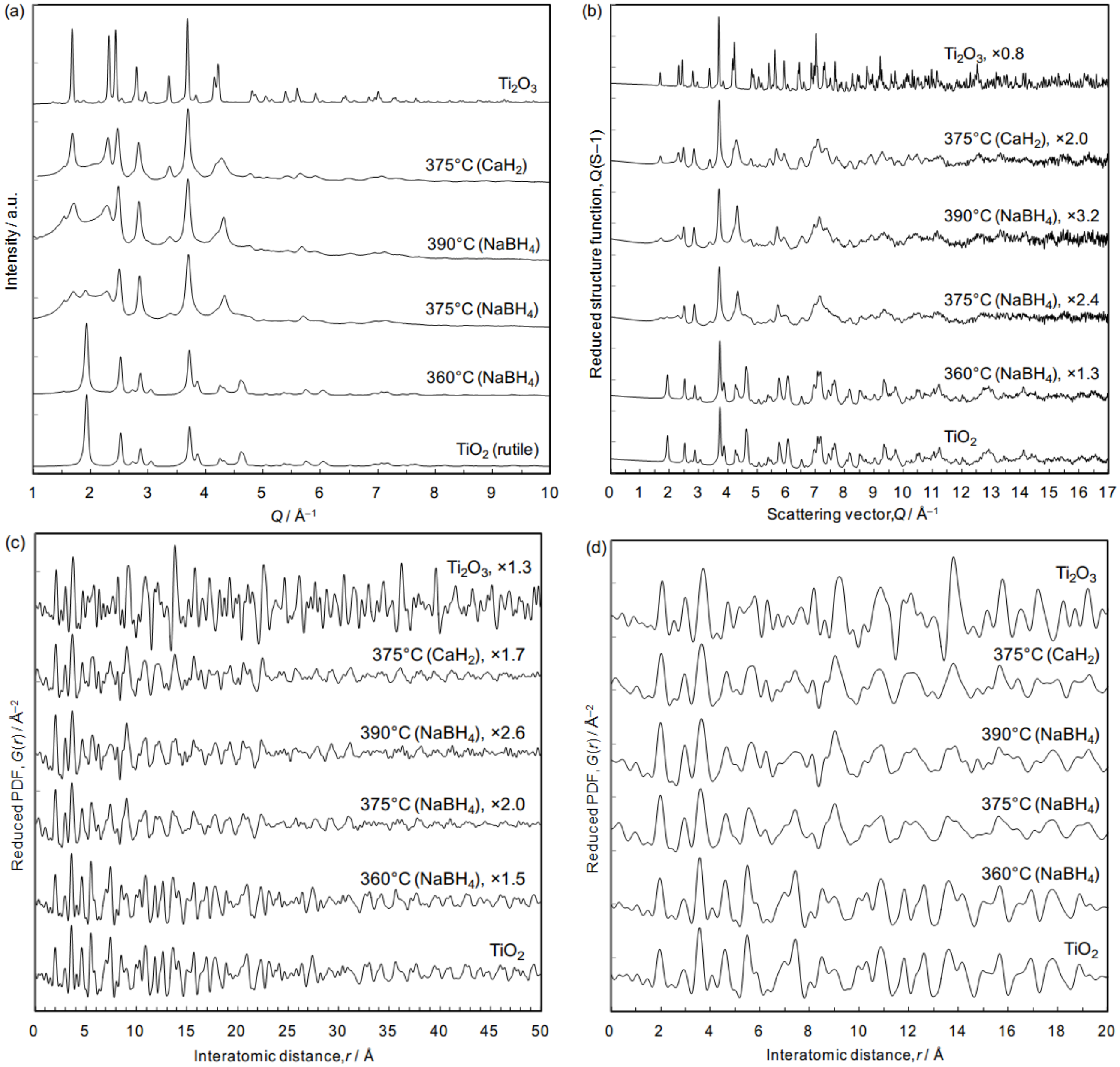

Fig. S1 Comparison of PDFs for rutile TiO_2 nanoparticles, those reduced under different conditions, and Ti_2O_3. (a) X-ray total scattering patterns collected on an imaging plate using a Mo Kα irradiation. (b) Reduced structure functions (scale, 20). (c, d) Pair distribution functions (scale, 20 $Å^{-2}$).

Total scattering data
TiO_2 nanoparticles reduced by CaH_2
Comparison of data obtained using Mo Ka and synchrotron

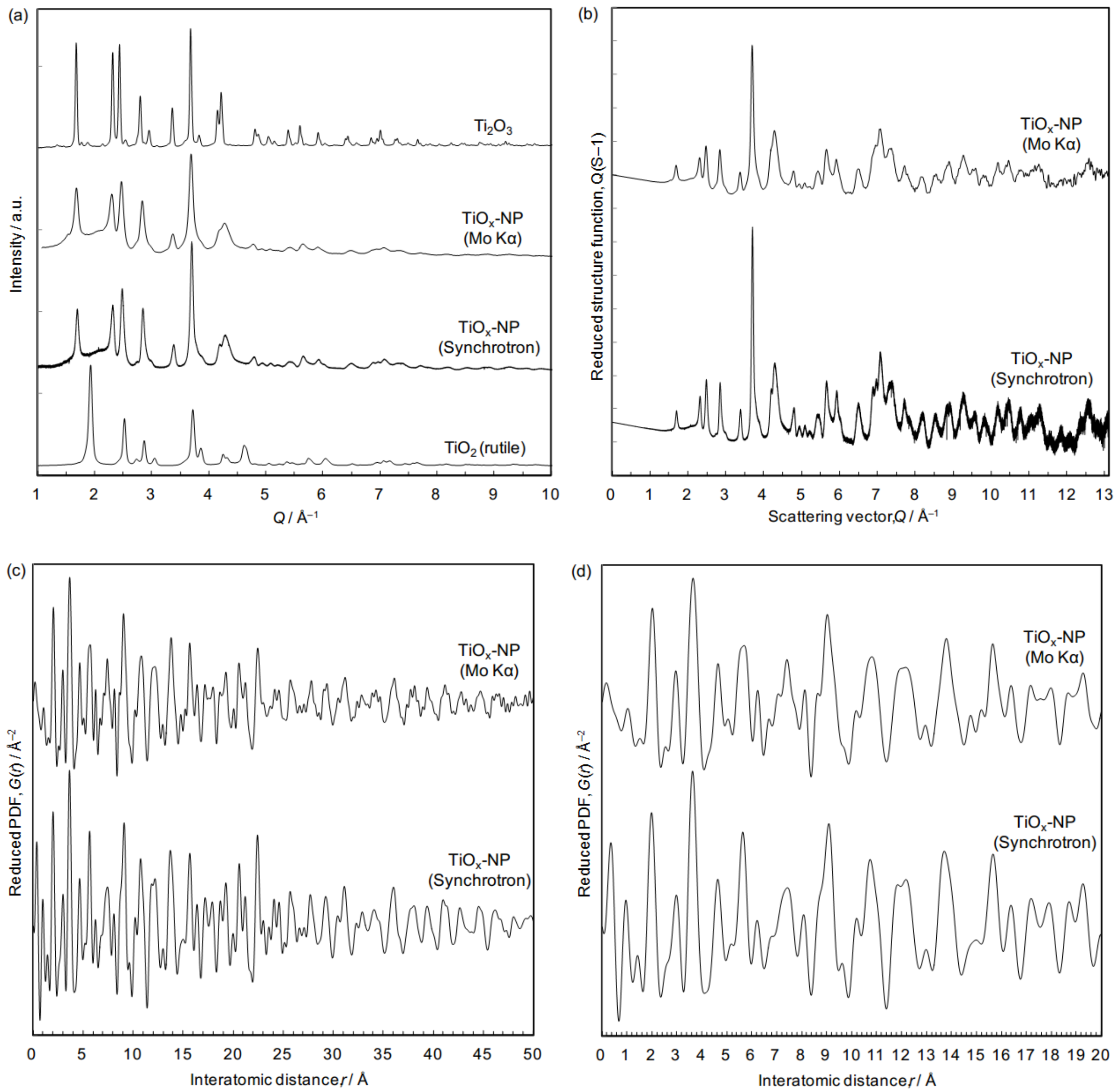

5 **Fig. S2** Comparison of TiO_x-NP's PDFs collected using a synchrotron X-ray and a Mo Kα irradiation. (a) X-ray total scattering patterns. (b) Reduced structure functions. (c, d) PDFs.

Total scattering data

TiO_2 nanorods reduced by $NaBH_4$

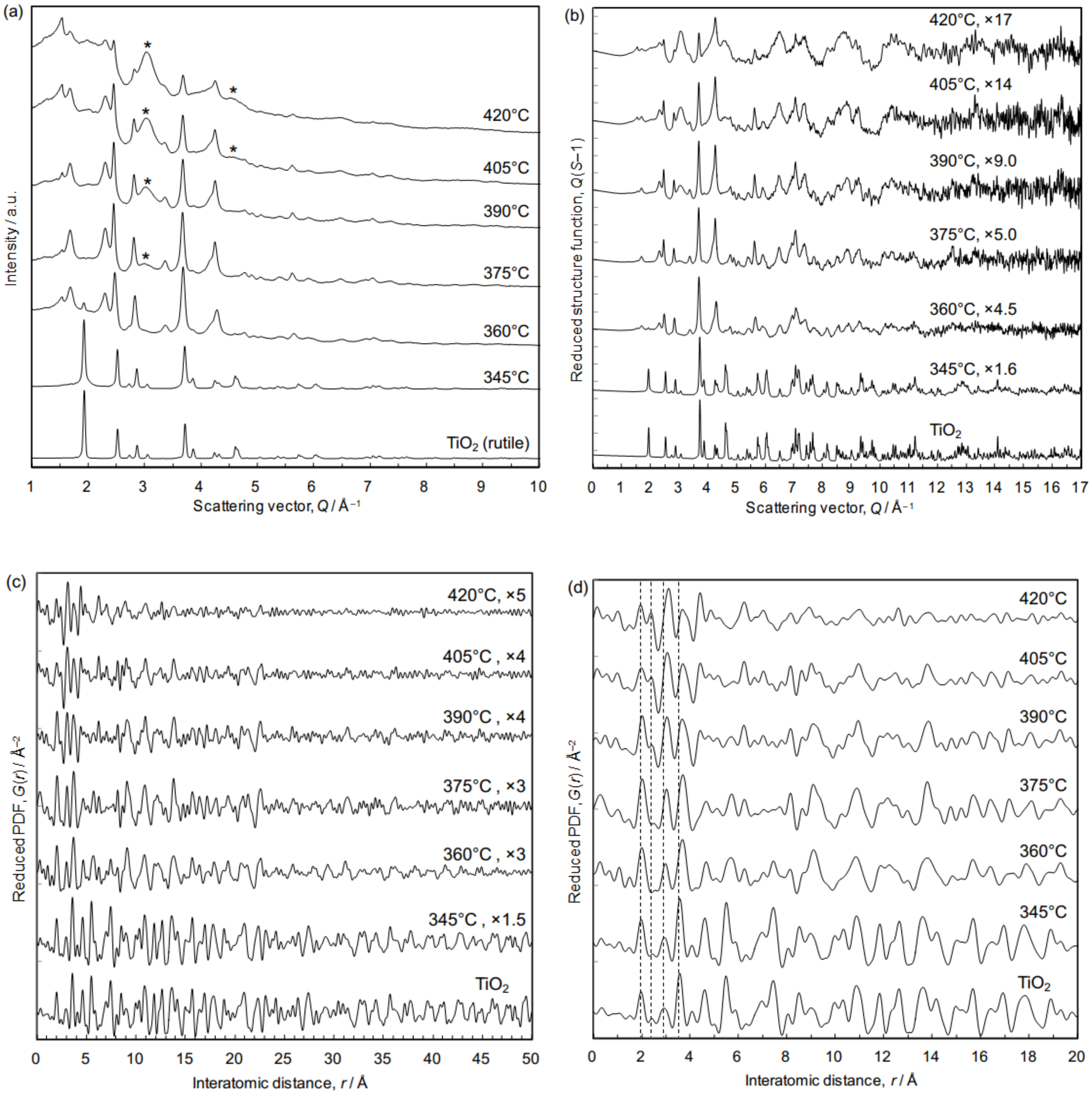

Fig. S3 Comparison of PDFs for rutile TiO_2 nanorods and those reduced using $NaBH_4$. (a) X-ray total scattering patterns. With increase of temperature, broad scattering peaks (*) are observed. (b) Reduced structure functions (scale, 20). (c, d) PDFs (scale, 20 $Å^{-2}$).

Calculated PDF patterns

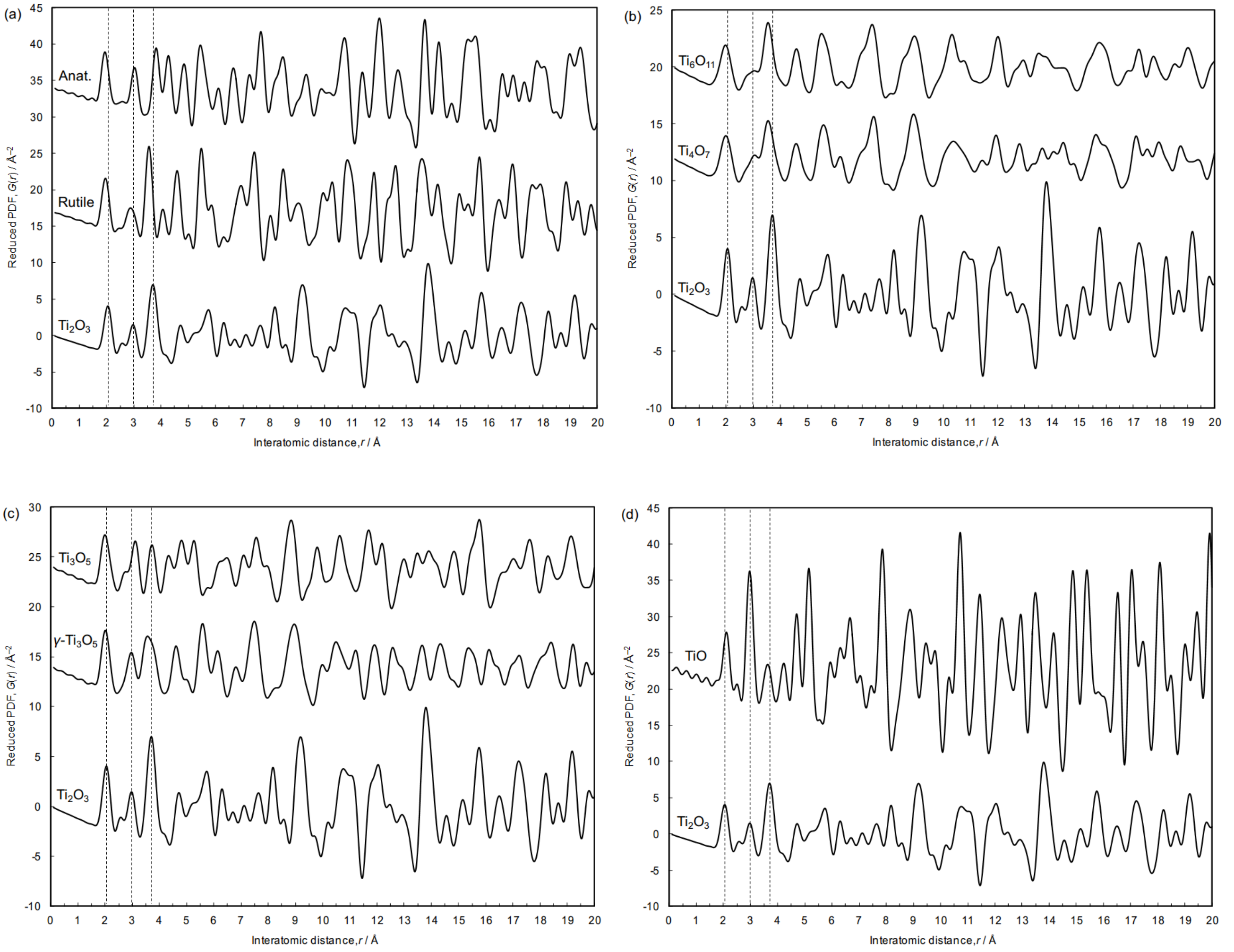

Fig. S4 Simulated PDFs. (a) Ti_2O_3 in $R\bar{3}c$ (ICSD no. 9646), rutile TiO_2 in $P4_2/mnm$ (ICSD no. 9161), anatase TiO_2 in $I4_1/amd$ (ICSD no. 9852). (b) Ti_4O_7 in $I\bar{1}$ (ICSD no. 48131) and Ti_6O_{11} in $I\bar{1}$ (ICSD no. 35121). (c) γ-Ti_3O_5 in $I12/c1$ (ICSD no. 35148) and Ti_3O_5 in $C12/m1$ (ICSD no. 26492). (d) TiO in $Fm\bar{3}m$ (ICSD no. 56612). U_{iso} for Ti is 0.005 and U_{iso} for O is 0.01.

Commercially available Ti_2O_3
Rietveld refinements

S3. Atomic structures of Ti_2O_3 particles

Table S1 Crystal structure data of Ti_2O_3 refined by the Rietveld method. R_{wp} = 4.11%, GOF ψ = 1.65.

Phase	**I**	**II**	**III**
Crystal phase	Ti_2O_3 (corundum)	γ-Ti_3O_5	Ti_3O_5
Space group	$R\bar{3}c$	$I12/c1$	$C12/m1$
Symmetry	Trigonal	Monoclinic	Monoclinic
Composition	Ti_2O_3	Ti_3O_5	Ti_3O_5
Phase fraction [a] (%)	79	11	10
a / Å	5.14966(9)	9.873(6)	9.739(5)
b / Å	= a	5.1384(19)	3.8085(13)
c / Å	13.6235(4)	7.123(7)	9.176(6)
β (°)	90	110.09(5)	93.63(5)
$U_{iso,Ti}$ / Å^2	0.00450(7)	0.00450(7)	0.00450(7)
$U_{iso,O}$ / Å^2	0.0084(5)	0.0084(5)	0.0084(5)
Ti1 (x, y, z)	0.0, 0.0, 0.34489(5)	0.3743(9), 0.498(6), 0.1472(16)	0.1463(20), 0.0, 0.0036(20)
Ti2 (x, y, z)	–	0.0, 0.5, 0.0	0.7728(17), 0.0, 0.1353(17)
Ti3 (x, y, z)	–	–	0.1269(18), 0.0, 0.5785(19)
O1 (x, y, z)	0.3043(4), 0.0, 0.25	0.808(4), 0.555(6), 0.682(9)	0.553(5), 0.0, 0.397(5)
O2 (x, y, z)	–	0.663(4), 0.339(6), 0.607(7)	0.215(6), 0.0, 0.420(5)
O3 (x, y, z)	–	0.0, 0.529(15), 0.25	0.557(5), 0.0, -0.128(5)
O4 (x, y, z)	–	–	0.677(5), 0.0, 0.165(5)
O5 (x, y, z)	–	–	0.974(4), 0.0, -0.316(4)
Ti–O	2.0316(15)		
Ti–O	2.0448(10)		
Ti–Ti	2.5855(14)		
Ti–Ti	2.98979(16)		
Particle size [b] / Å	937	937	263

[a] calculated from refined values of unit cell fractions. [b] calculated from (18000*K*λ)/(π*LX), where LX is the Lorentzian isotropic crystallite size broadening term, λ is the wavelength (0.7107), and K is the Scherrer constant (1.0).

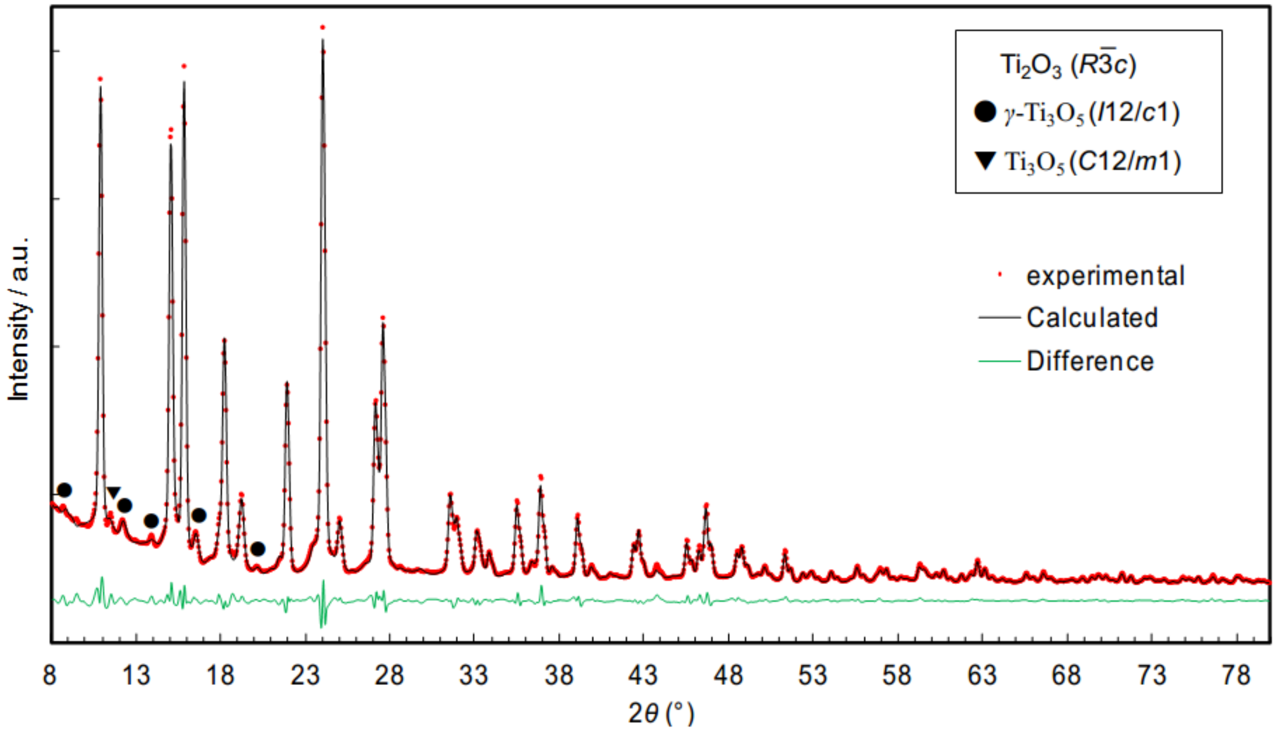

Fig. S5 Rietveld refinements of powder X-ray diffraction pattern of Ti_2O_3.

Commercially available Ti_2O_3
PDF refinements in different *r* ranges (10 Å pitch)

Table S2 Atomic structure data obtained by PDF refinements for Ti_2O_3

Fitting range	0.01–10 Å	10–20 Å	20–30 Å	30–40 Å	40–50 Å	0.01–50 Å	XRD
R_w (%)	14.4984	11.7751	12.4752	17.0372	30.1115	20.0656	GOF 1.65
Space group	$R\bar{3}c$	$R\bar{3}c$	$R\bar{3}c$	$R\bar{3}c$	$R\bar{3}c$	$R\bar{3}c$	$R\bar{3}c$
Composition	Ti_2O_3	Ti_2O_3	Ti_2O_3	Ti_2O_3	Ti_2O_3	Ti_2O_3	Ti_2O_3
a / Å	5.15485	5.15734	5.15611	5.1579	5.16226	5.15858	5.14966(9)
	(2.6e-007)	(1.1e-007)	(1.1e-007)	(8.6e-008)	(9.2e-008)		
b / Å	= *a*	= *a*	= *a*	= *a*	= *a*	= *a*	= *a*
c / Å	13.6292	13.6385	13.6419	13.6337	13.6605	13.6419	13.6235(4)
	(1.8e-006)	(5.5e-007)	(5.4e-007)	(6.2e-007)	(5.7e-007)	(1.7e-007)	
$U_{iso,Ti}$ / Å^2	0.0005928	0.00105206	0.00303307	0.00531482	0.00408152	0.00266715	0.00450(7)
	(4.6e-008)	(3.6e-008)	(4.4e-008)	(5e-008)	(6e-008)	(1.5e-008)	
$U_{iso,O}$ / Å^2	0.0112448	0.00911542	0.0103457	0.0118549	0.0348195	0.0099816	0.0084(5)
	(1.9e-007)	(1.6e-007)	(2.1e-007)	(2.3e-007)	(7.1e-007)	(6.8e-008)	
Particle diameter / Å	–[a]	–[a]	–[a]	–[a]	–[a]	111.55	–

[a] Fixed to 111.55 Å.

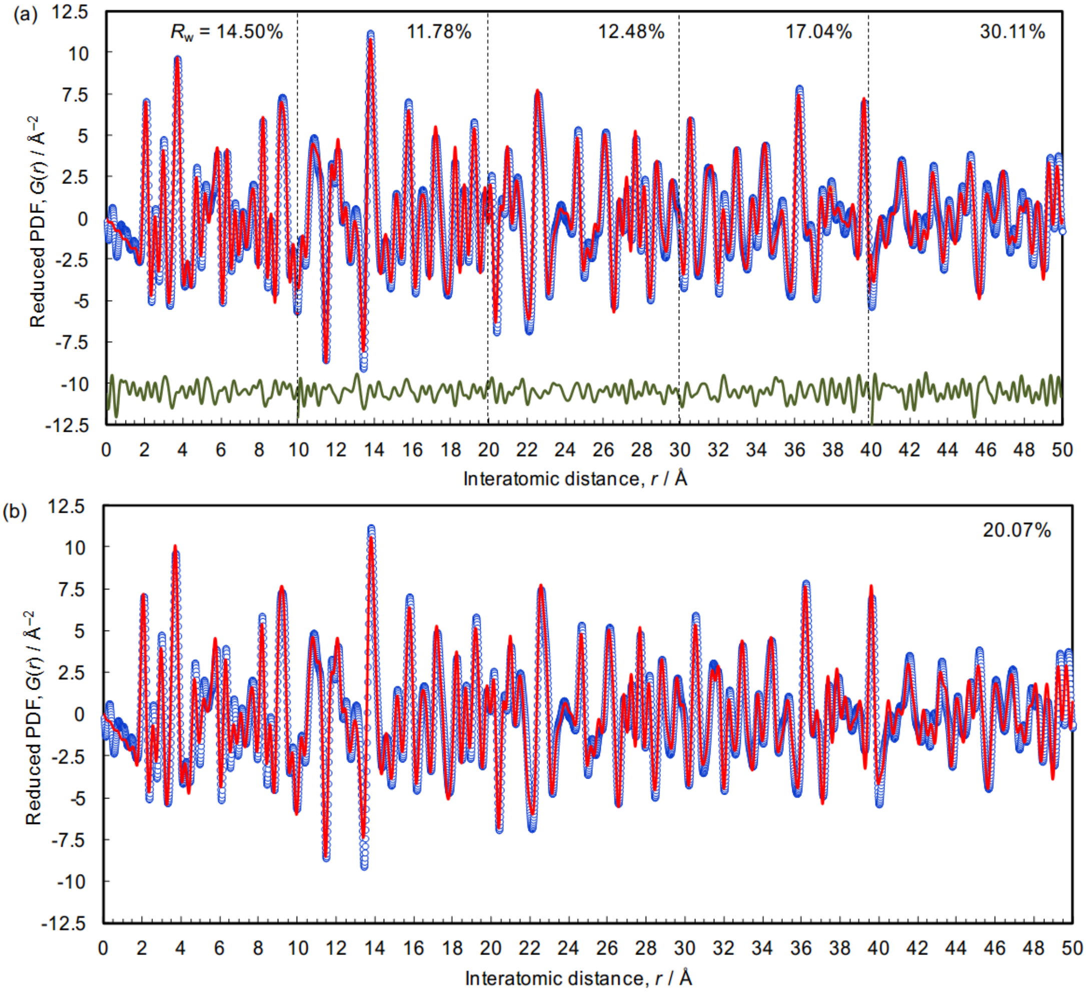

Fig. S6 PDF refinements of Ti_2O_3. (a) Refinements at every 10 Å. (b) Refinement in the range from 0 to 50 Å. Experimental PDF plots (blue dots) with calculated ones based on corundum Ti_2O_3 (red line). Their difference is at the bottom (green curve).

TiO_2 nanoparticles
Rietveld refinements

S4. Atomic structures of TiO_2 nanoparticles

Table S3 Atomic structure data refined by the Rietveld method for rutile TiO_2 nanoparticles and nanorods.

Sample	TiO_2 nanoparticles	TiO_2 nanorods
Refinement	Diffraction (Rietveld)	Diffraction (Rietveld)
R_{wp} (%), ψ	3.94, GOF 1.64	4.42, 1.82
Fitting range	10–80° (2θ)	8–80° (2θ)
Space group	$P4_2/mnm$	$P4_2/mnm$
a / Å	4.59106(23)	4.59218(12)
c / Å	2.95334(22)	2.95806(12)
$U_{iso,Ti}$ / Å^2	0.02249(16)	0.02062(15)
$U_{iso,O}$ / Å^2	0.0201(6)	0.0275(6)
Ti(x)	0.0	0.0
Ti(y)	0.0	0.0
Ti(z)	0.0	0.0
O(x)	0.30559(31)	0.30754(32)
O(y)	0.30559(31)	0.30754(32)
O(z)	0.0	0.0
Particle size[a] / Å	120	795

[a] calculated from (18000*K*λ)/(π*LX), where LX is the Lorentzian isotropic crystallite size broadening term, λ is the wavelength (0.7107), and K is the Scherrer constant (1.0).

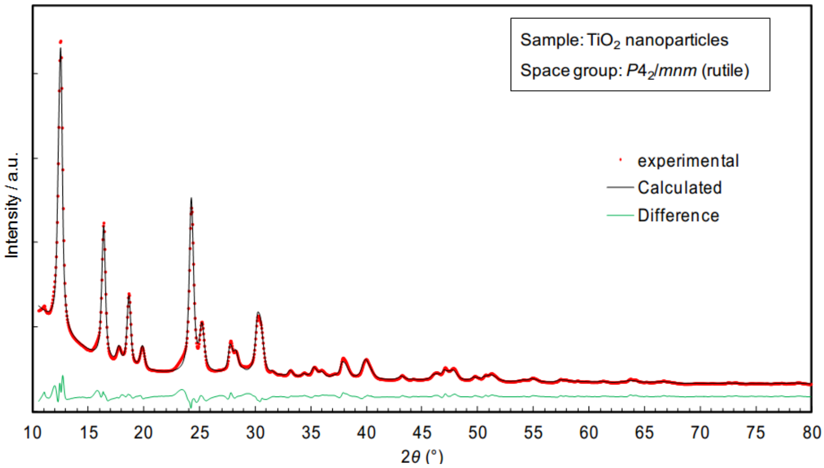

Fig. S7 Rietveld refinement of powder X-ray diffraction pattern of rutile TiO_2 nanoparticles.

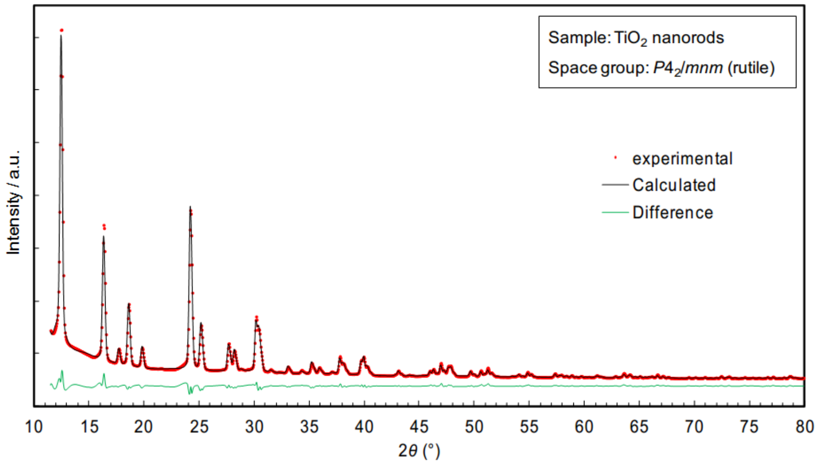

Fig. S8 Rietveld refinement of powder X-ray diffraction pattern of rutile TiO_2 nanorods.

Rutile TiO_2 nanoparticles
PDF refinements in different *r* ranges (10 Å pitch)

Table S4 Atomic structure data obtained by PDF refinements for rutile TiO_2 nanoparticles

Fitting range	0.01–10 Å	10–20 Å	20–30 Å	30–40 Å	40–50 Å	0.01–50 Å	XRD
R_w (%)	12.1719	12.3814	14.0815	18.5736	21.8566	17.1866	GOF 1.64
Space group	*P*4$_2$/*mnm*	*P*4$_2$/*mnm*	*P*4$_2$/*mnm*	*P*4$_2$/*mnm*	*P*4$_2$/*mnm*	*P*4$_2$/*mnm*	*P*4$_2$/*mnm*
Composition	TiO_2	TiO_2	TiO_2	TiO_2	TiO_2	TiO_2	TiO_2
a / Å	4.60256 (5.6e-007)	4.59494 (2.2e-007)	4.59585 (1.9e-007)	4.59775 (2.4e-007)	4.59742 (2.8e-007)	4.59641 (9.1e-008)	4.59106(23)
c / Å	2.95814 (6.6e-007)	2.95832 (2.7e-007)	2.95581 (2.6e-007)	2.95607 (2.4e-007)	2.95523 (2.6e-007)	2.9573 (9.8e-008)	2.95334(22)
$U_{iso,Ti}$ / Å^2	0.00703396 (7.7e-008)	0.0105657 (2.1e-007)	0.0107031 (1.6e-007)	0.0149928 (4.1e-007)	0.0170883 (5.4e-007)	0.00901257 (5.2e-008)	0.02249(16)
$U_{iso,O}$ / Å^2	0.00728996 (2.8e-007)	0.0168989 (5.6e-007)	0.0184911 (9.4e-007)	0.0122696 (9e-007)	0.0110863 (1.1e-006)	0.0119734 (2.1e-007)	0.0201(6)
Particle diameter / Å	–[a]	–[a]	–[a]	–[a]	–[a]	76.7789	–

[a] Fixed to 76.7789.

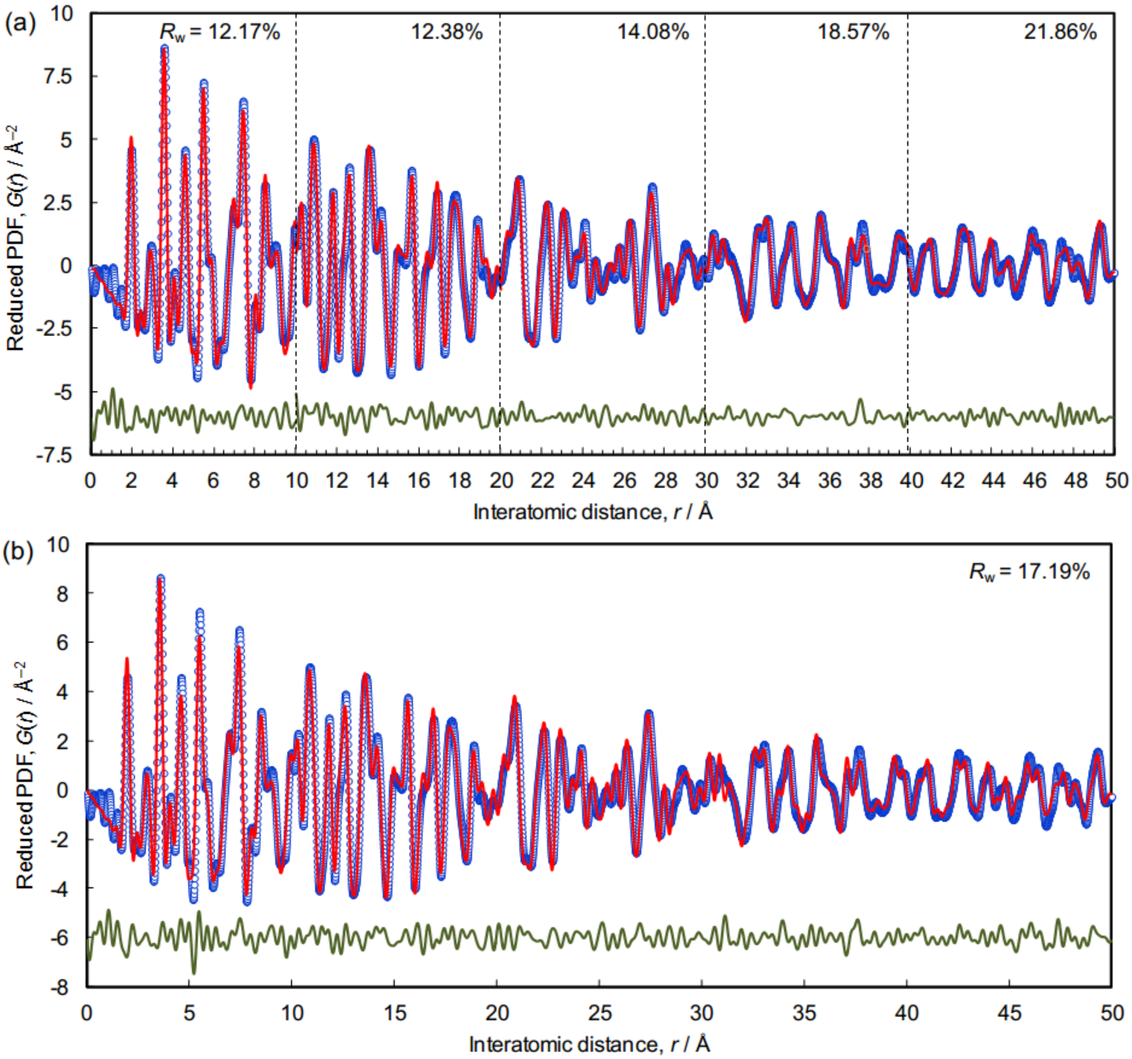

Fig. S9 PDF refinement of TiO_2 nanoparticles. (a) Refinements at every 10 Å. (b) Refinement in the range from 0 to 50 Å. Experimental PDF plots (blue dots) with calculated ones based on rutile TiO_2 (red line). Their difference is at the bottom (green curve).

Rutile TiO_2 nanorods
PDF refinements in different *r* ranges (10 Å pitch)

Table S5 Atomic structure data of TiO_2 nanorods obtained by PDF refinements.

Fitting range R_w (%)	0.01–10 Å 11.9346	10–20 Å 10.5244	20–30 Å 14.3483	30–40 Å 17.6302	40–50 Å 26.707	0.01–50 Å 18.1291	XRD GOF 1.82
a / Å	4.60194 (5.6e-007)	4.59869 (1.6e-007)	4.598 (1.2e-007)	4.59998 (1.4e-007)	4.60081 (1.3e-007)	4.59959 (5.8e-008)	4.59218(12)
c / Å	2.96158 (6.1e-007)	2.96286 (2.1e-007)	2.96068 (1.7e-007)	2.96207 (1.2e-007)	2.96241 (1.1e-007)	2.96304 (5.8e-008)	2.95806(12)
$U_{iso,Ti}$ / $Å^2$	0.00496118 (6.7e-008)	0.00829168 (1.5e-007)	0.00884875 (3.8e-007)	0.0127743 (5.8e-007)	0.0231604 (1.1e-006)	0.00697025 (3.4e-008)	0.02062(15)
$U_{iso,O}$ / $Å^2$	0.00773422 (3.2e-007)	0.0166404 (4.9e-007)	0.0166269 (1.1e-006)	0.0200465 (1.2e-006)	0.0137994 (1e-006)	0.0138693 (2.2e-007)	0.0275(6)
Particle diameter / Å	–[a]	–[a]	–[a]	–[a]	–[a]	119.835	–

[a] Fixed to 119.835 Å.

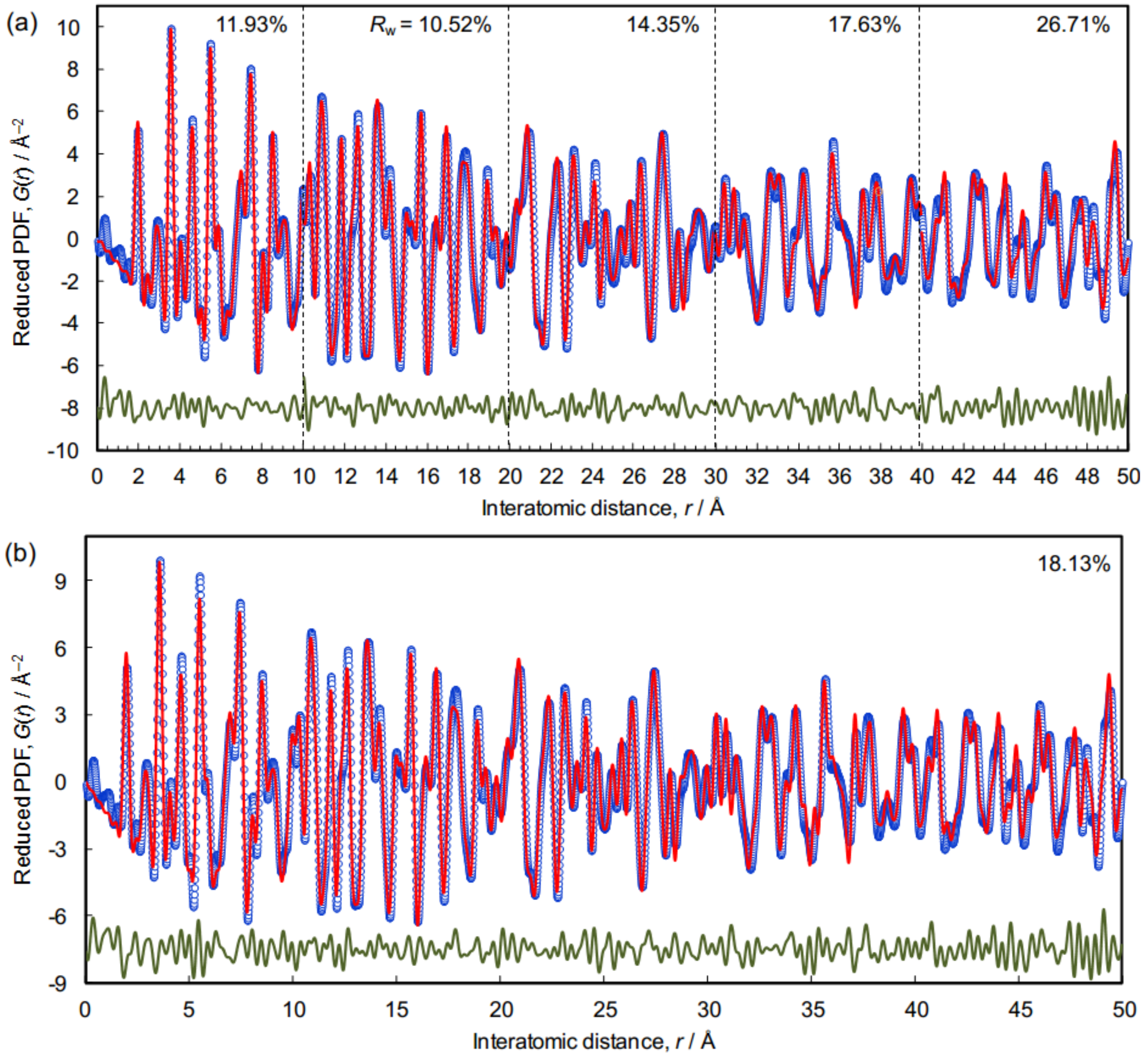

Fig. S10 PDF refinement of TiO_2 nanorods. (a) Refinements at every 10 Å. (b) Refinement in the range from 0 to 50 Å. Experimental PDF plots (blue dots) with calculated ones based on rutile TiO_2 (red line). Their difference is at the bottom (green curve).

S5. Atomic structure of TiO_2 nanoparticles reduced by CaH_2, "TiO_x-NP"

As is often the way with crystalline particles, crystal structures of TiO_x-NP were analyzed by X-ray diffraction, and the Bragg peaks are assignable to a corundum structure. Considering the relatively low reaction temperature, Ti deficiency may be ordered. Thus, the crystal structure in three rhombohedral space groups of corundum ($R\bar{3}c$), ilmenite-type ($R\bar{3}$) and $LiNbO_3$-type structure ($R3c$), assuming ordering of Ti deficiency in one of two Ti sites in the latter two structures as illustrated in Fig. S11.

Judging from the goodness-of-fit values ($R\bar{3}c$, 1.44; $R\bar{3}$, 1.37; $R3c$, 1.58), ilmenite-type structure having ordered Ti deficiency in a Ti site is more reasonable than the corundum structure having uniform distribution of Ti deficiency. The Ti occupancy in the ilmenite-type structure is 61%, which corresponds to 81% of Ti occupancy in the whole structure, and reasonably corresponds to the composition determined by TGA. Unless there are phases undetectable by X-ray diffraction, this analysis is considered to be correct, but the conventional diffraction technique should not be trusted blindly for nanomaterials.

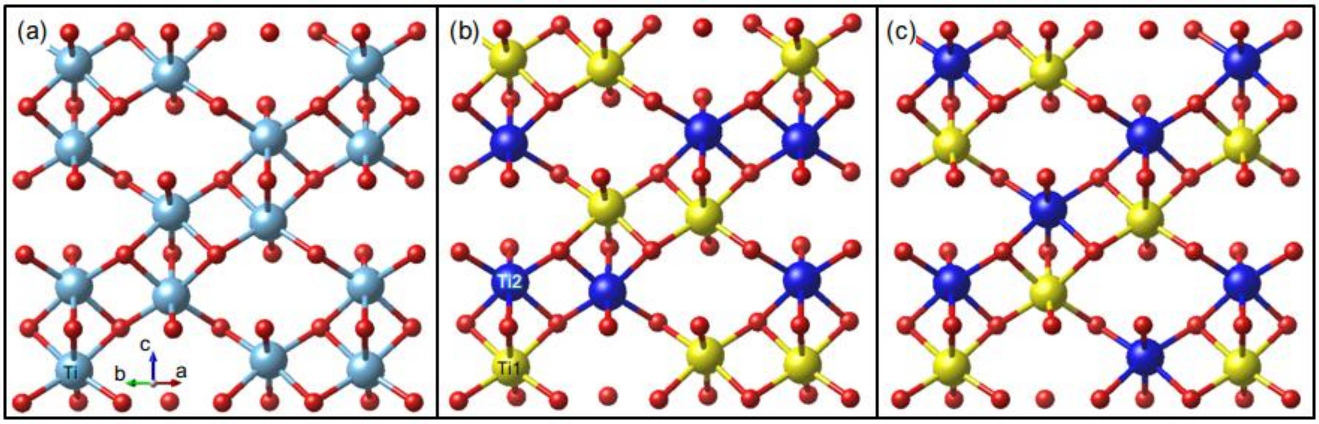

Fig. S11 Illustration representing the difference of Ti sites among Ti_2O_3 in $R\bar{3}c$ (a), in $R\bar{3}$ (b) and $R3c$ (c).

Table S6 Atomic structure data for TiO_x-NP refined by the Rietveld method. I–III, occupancy is fixed to be 1.0. IV–VI, occupancy of Ti1 was refined.

Refinement no.	**I**	**II**	**III**	**IV**	**V**	**VI**
Crystal type	Corundum	Ilmenite	$LiNbO_3$	Corundum	Ilmenite	$LiNbO_3$
Space group	$R\bar{3}c$	$R\bar{3}$	$R3c$	$R\bar{3}c$	$R\bar{3}$	$R3c$
Ideal composition	Ti_2O_3	Ti_2O_3	Ti_2O_3	Ti_2O_3	Ti_2O_3	Ti_2O_3
Refined composition	Ti_2O_3	Ti_2O_3	Ti_2O_3	$Ti_{1.81}O_3$	$Ti_{1.61}O_3$	$Ti_{1.76}O_3$
R_{wp} (%)	5.73	5.94	6.10	5.21	4.95	5.73
GOF = ψ	1.58	1.64	1.68	1.44	1.37	1.58
a / Å	5.0591(5)	5.0563(6)	5.0638(6)	5.0528(5)	5.0569(5)	5.0638(6)
b / Å	= a	= a	= a	= a	= a	= a
c / Å	13.7312(19)	13.7525(19)	13.7633(20)	13.7306(17)	13.7590(16)	13.7707(19)
$U_{iso,Ti}$ / Å^2	0.00487(13)	0.00288(12)	0.00186(11)	0.00848(14)	0.00370(10)	0.00265(11)
$U_{iso,O}$ / Å^2	$U_{iso,Ti}$ ×2	$U_{iso,Ti}$ ×2	$U_{iso,Ti}$ ×2	$U_{iso,Ti}$ ×2	$U_{iso,Ti}$ ×2	$U_{iso,Ti}$ ×2
Occupancy, Ti1	1.0	1.0	1.0	0.8068(16)	0.6112(29)	0.758(4)
Occupancy, Ti2	–[a]	1.0	1.0	–[a]	1.0	1.0
Ti1(z)	0.34044(12)	0.33952(25)	0.31826(26)	0.34021(12)	0.34117(27)	0.31692(28)
Ti2(z)	–[a]	0.15844(25)	0.0	–[a]	0.16039(17)	-0.00123(13)
O(x)	0.3331(9)	0.3279(10)	0.3293(21)	0.3335(7)	0.3102(7)	0.3262(12)
O(y)	0.0	–0.0121(18)	–0.0009(18)	0.0	-0.0456(8)	0.0038(24)
O(z)	0.25	0.2478(13)	0.2348(9)	0.25	0.2486(4)	0.23865(25)
<u>Nearest neighbour distance</u>						
Ti1–O	1.9853(21), 2.093(4)	1.968(13), 2.109(12)	2.027(12), 2.050(10)	1.9842(17), 2.0916(29)	1.850(5), 2.121(5)	1.964(8), 2.088(7)
Ti2–O	–[a]	1.999(10), 2.089(12)	1.936(11), 2.175(10)	–[a]	2.085(5), 2.133(4)	1.999(11), 2.130(6),
Ti1–Ti1 /Å	2.4837(34), 2.9274(4)	2.9242(5)	–	2.4773(33), 2.9234(4)	2.9276(6)	–
Ti1–Ti2 /Å	–[a]	2.490(5)	2.501(4), 2.9309(4)	–[a]	2.487(4)	2.504(5), 2.9310(5)
Ti2–Ti2 /Å	–[a]	2.9280(6)	–	–[a]	2.9247(4)	–

[a] Ti(1) = Ti(2).

Rutile TiO_2 nanoparticles reduced by CaH_2
Crystal structure refined by the Rietveld method in three rhombohedral space groups

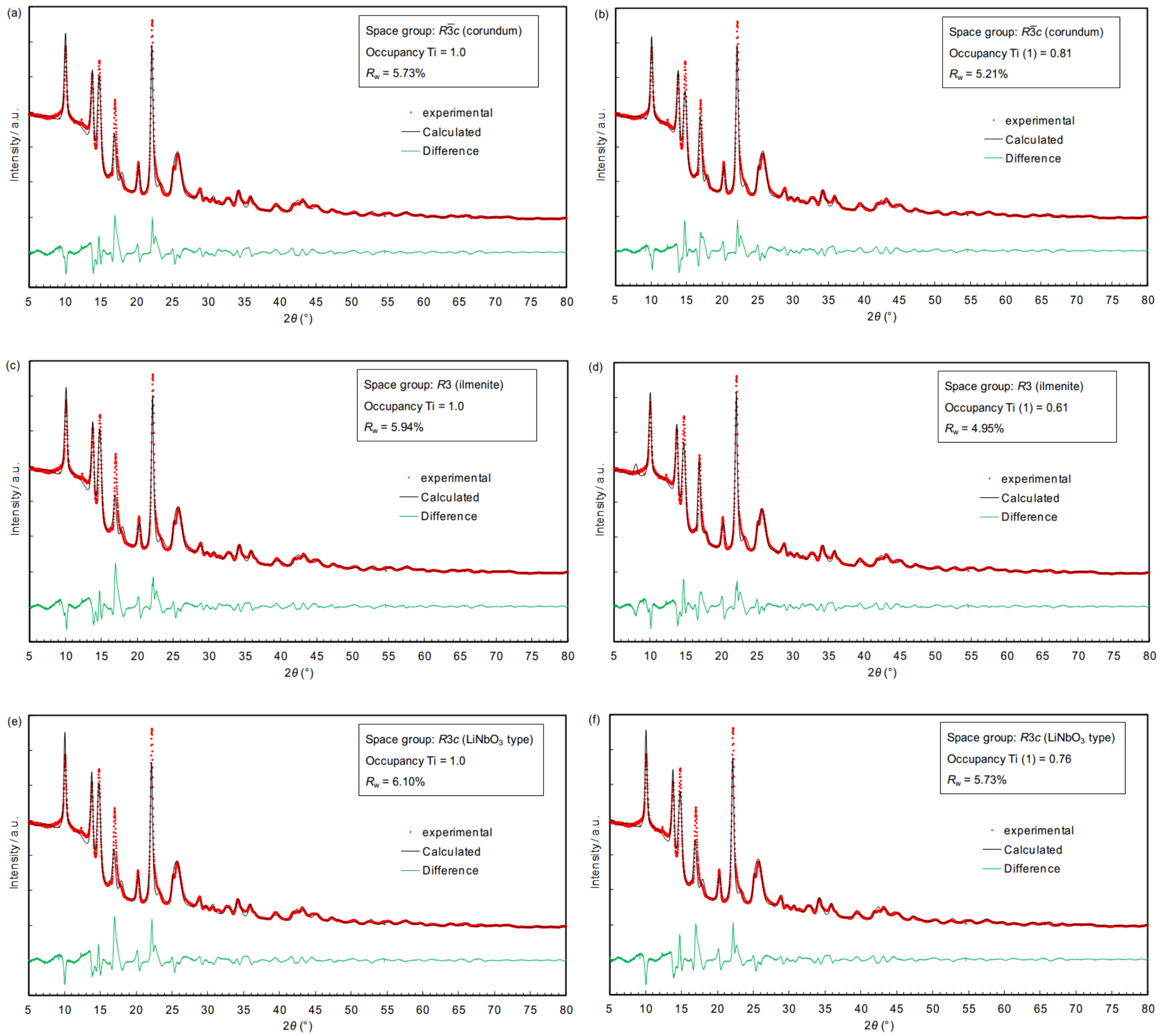

Fig. S12 Rietvelt refinements of the powder XRD patterns of TiO_x-NP: corundum structure in space group $R\bar{3}c$ without (a) and with (b) Ti occupancy refinement; ilmenite-type structure in $R\bar{3}$ without (c) and with (d) Ti occupancy refinement; and $LiNbO_3$-type structure in $R3c$ without (e) and with (f) Ti occupancy refinement.

Rutile TiO_2 nanoparticles reduced by CaH_2
Atomic structure analyzed by the PDF refinements (summary)

Table S7 Atomic structure data of TiO_x-NP analyzed by the PDF refinements within 30 Å.

Model	Ti_2O_3 only	$Ti_2O_3 + TiO_2$		$Ti_2O_3 + Ti_4O_7$		$Ti_2O_3 + Ti_5O_9$		$Ti_2O_3 + Ti_6O_{11}$	
R_w (%)	38.5597	35.0502		23.5052		27.0113		24.3367	
Phase	Ti_2O_3	Ti_2O_3	TiO_2	Ti_2O_3	Ti_4O_7	Ti_2O_3	Ti_5O_9	Ti_2O_3	Ti_6O_{11}
Space group	$R\bar{3}c$	$R\bar{3}c$	$P4_2/mnm$	$R\bar{3}c$	$I\bar{1}$	$R\bar{3}c$	$P\bar{1}$	$R\bar{3}c$	$I\bar{1}$
a / Å	5.07236 (7e-007)	5.08358 (8.1e-007)	4.6937 (3.8e-006)	5.09391 (7.3e-007)	5.42228 (5e-006)	5.09047 (7.9e-007)	5.47004 (4.1e-006)	5.08719 (7.5e-007)	5.46333 (6.9e-006)
b / Å	$= a$	$= a$	$= a$	$= a$	7.34652 (6.4e-006)	$= a$	7.3341 (5e-006)	$= a$	7.30065 (7.4e-006)
c / Å	13.8088 (2.7e-006)	13.7733 (3.3e-006)	2.97789 (4.2e-006)	13.7947 (4.1e-006)	20.1786 (1.7e-005)	13.7926 (4e-006)	8.88012 (7.6e-006)	13.8231 (4.1e-006)	31.992 (3.6e-005)
α (°)	90	90	90	90	66.4063 (7.1e-005)	90	101.637 (6.2e-005)	90	67.109 (0.00011)
β (°)	90	90	90	90	58.1005 (7.6e-005)	90	111.53 (5.2e-005)	90	57.704 (8.5e-005)
γ (°)	120	120	90	120	108.257 (6.9e-005)	120	108.107 (6e-005)	120	109.001 (9.5e-005)
$U_{iso,Ti}$ / Å^2	0.0152577 (1.7e-007)	0.0134509 (2.6e-007)	0.0163045 (1.2e-006)	0.00791217 (1.3e-007)	0.00791217 (1.3e-007)	0.0100485 (1.9e-007)	0.0100485 (1.9e-007)	0.00867751 (1.1e-007)	0.00867751 (1.1e-007)
$U_{iso,O}$ / Å^2	0.0230208 (6.1e-007)	0.0219631 (8e-007)	0.00574147 (1.2e-006)	0.0164582 (5.3e-007)	0.0164582 (5.3e-007)	0.0152363 (5.4e-007)	0.0152363 (5.4e-007)	0.014101 (4.4e-007)	0.014101 (4.4e-007)
Particle diameter / Å	46.7782	–[a]	–[a]	59.878	55.5969	52.3854	321.133	48.4561	118.717
Phase content [b]	–	0.73385	0.26615	0.530598	0.469402	0.684154	0.315846	0.564708	0.435292

[a] Large enough value was used but it is not meaningful. [b] Relative phase content in terms of atoms.

Atomic structure analyzed by the PDF refinements in different *r* ranges (10 Å pitch)

1. Ti_2O_3 / Mixed phases of Ti_2O_3 and TiO_2

Table S8 Atomic structure data of TiO_x-NP analyzed by the PDF refinements (Ti_2O_3 or Ti_2O_3+TiO_2).

Fitting range	0.01–10 Å	0.01–30 Å	0.01–10 Å		0.01–30 Å		XRD
R_w (%)	32.336	38.5597	21.5601		30.5168		GOF 1.58
	Ti_2O_3	Ti_2O_3	Ti_2O_3	TiO_2	Ti_2O_3	TiO_2	Ti_2O_3
a / Å	5.05256 (1.4e-006)	5.07236 (7e-007)	5.1079 (2.7e-006)	4.74741 (4.8e-006)	5.08354 (6.7e-007)	4.71731 (2e-006)	5.0591(5)
b / Å	= *a*	= *a*	= *a*	= *a*	= *a*	= *a*	= *a*
c / Å	13.7877 (8.4e-006)	13.8088 (2.7e-006)	13.6848 (1.5e-005)	2.86424 (3.8e-006)	13.7907 (3.9e-006)	2.84643 (2.1e-006)	13.7312(19)
$U_{iso,Ti}$ / Å^2	0.0101869 (2.3e-007)	0.0152577 (1.7e-007)	0.00557481 (2e-007)	0.00557481 (2e-007)	0.00870404 (1.7e-007)	0.00870404 (1.7e-007)	0.00487(13)
$U_{iso,O}$ / Å^2	0.0197725 (1.1e-006)	0.0230208 (6.1e-007)	0.0111455 (6e-007)	0.0111455 (6e-007)	0.0191377 (5.5e-007)	0.0191377 (5.5e-007)	$U_{iso,Ti}$ ×2
Particle diameter / Å	–[a]	46.7782	–[a]	–[a]	46.7569	41.2924	–
Phase content [b]	–	–	0.723247	0.276753	0.768443	0.231557	–

[a] Large enough value was used but it is not meaningful. [b] Relative phase content in terms of atoms. [c] fixed, otherwise not converged well.

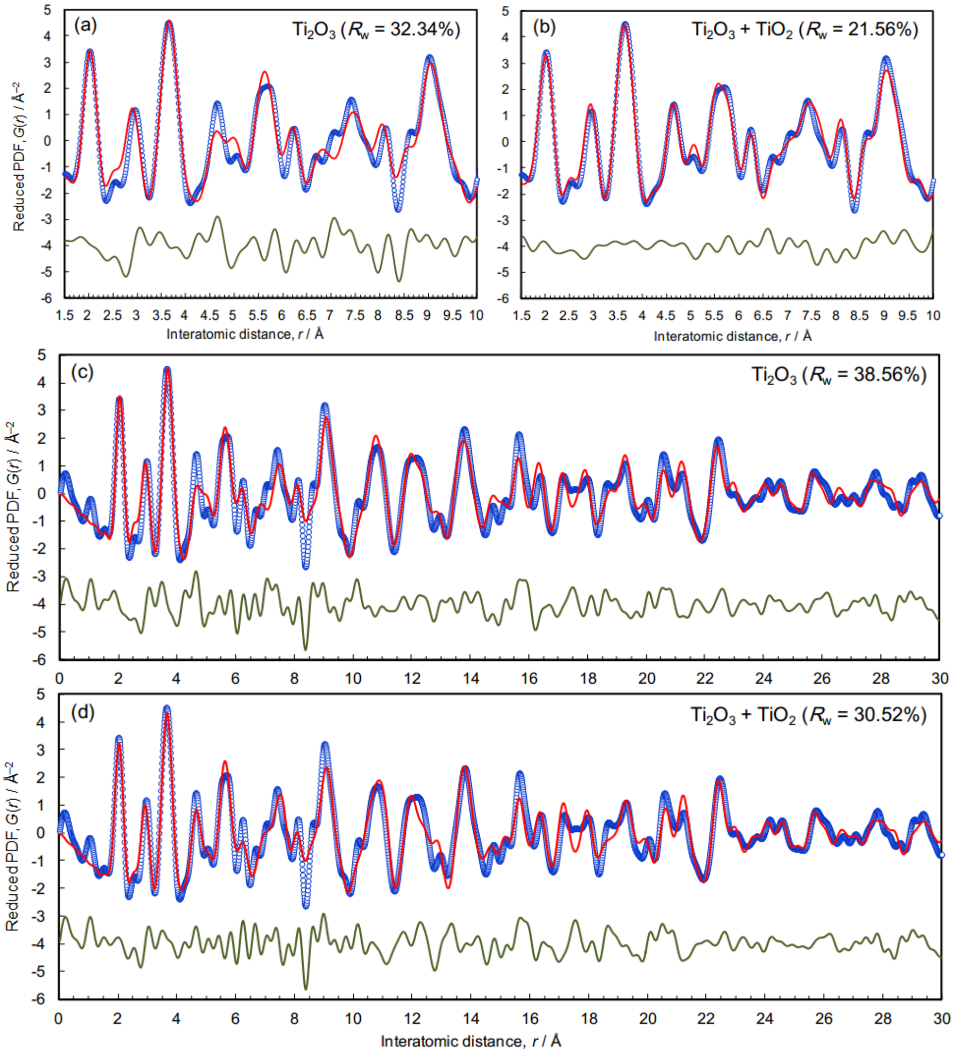

Fig. S13 PDF refinements of TiO_x-NP. (a, c) Corundum Ti_2O_3 only. (b, d) Corundum Ti_2O_3 + rutile TiO_2. Experimental PDF plots (blue dots) with calculated ones based on corundum Ti_2O_3 (red line). Their difference is at the bottom (green curve).

Rutile TiO_2 nanoparticles reduced by CaH_2
Atomic structure analyzed by the PDF refinements in different *r* ranges (10 Å pitch)
2. Mixed phases of Ti_2O_3 and Ti_4O_7

Table S9 Atomic structure data of TiO_x-NP analyzed by PDF refinements (Ti_2O_3+Ti_4O_7).

Fitting range	0.01–10 Å		10–20 Å		20–30 Å		30–40 Å		0.01–30 Å	
R_w (%)	19.9366		19.0107		18.2425		33.1388		23.5052	
	Ti_2O_3 $R\bar{3}c$	Ti_4O_7 $I\bar{1}$	Ti_2O_3 $R\bar{3}c$	Ti_4O_7 $I\bar{1}$	Ti_2O_3 $R\bar{3}c$	Ti_4O_7 $I\bar{1}$	Ti_2O_3 $R\bar{3}c$	Ti_4O_7 $I\bar{1}$	Ti_2O_3 $R\bar{3}c$	Ti_4O_7 $I\bar{1}$
a / Å	5.09084 (4.1e-006)	5.36516 (8.7e-006)	5.09817 (1.7e-006)	5.40318 (7.6e-006)	5.09056 (2.5e-006)	5.48298 (1.5e-005)	5.08777 (8.6e-006)	5.4268 (7.5e-005)	5.09391 (7.3e-007)	5.42228 (5e-006)
b / Å	= *a*	7.32304 (1.1e-005)	= *a*	7.32447 (1.7e-005)	= *a*	7.29982 (1.6e-005)	= *a*	7.40894 (7.8e-005)	= *a*	7.34652 (6.4e-006)
c / Å	13.8557 (1.7e-005)	20.2091 (4.9e-005)	13.8258 (1e-005)	20.3229 (3.2e-005)	13.7772 (9e-006)	19.9442 (4.7e-005)	13.7527 (1.7e-005)	19.9449 (0.00022)	13.7947 (4.1e-006)	20.1786 (1.7e-005)
α (°)	90	65.8544 (0.0002)	90	66.4871 (0.00012)	90	67.7144 (0.00024)	90	66.821 (0.0012)	90	66.4063 (7.1e-005)
β (°)	90	58.9303 (0.00012)	90	57.865 (0.00017)	90	57.6709 (0.00018)	90	58.5575 (0.00085)	90	58.1005 (7.6e-005)
γ (°)	120	107.868 (0.00018)	120	108.253 (0.00016)	120	108.909 (0.00027)	120	108.813 (0.00094)	120	108.257 (6.9e-005)
$U_{iso,Ti}$	0.00484234 (1.9e-007)	0.00484234 (1.9e-007)	0.00785057 (2.8e-007)	0.00785057 (2.8e-007)	0.0121119 (8.1e-007)	0.0121119 (8.1e-007)	0.0299446 (2.3e-006)	0.0299446 (2.3e-006)	0.00791217 (1.3e-007)	0.00791217 (1.3e-007)
$U_{iso,O}$	0.0187193 (9e-007)	0.0187193 (9e-007)	0.0177425 (1.3e-006	0.0177425 (1.3e-006)	0.0185114 (2.2e-006)	0.0185114 (2.2e-006)	0.0734907 (2.3e-005)	0.0734907 (2.3e-005)	0.0164582 (5.3e-007)	0.0164582 (5.3e-007)
Particle diameter / Å	–[a]	–[a]	–[a]	–[a]	–[a]	–[a]	–[a]	–[a]	59.878	55.5969
Phase content [b]	0.468801	0.531199	0.527431	0.472569	0.522227	0.477773	0.518529	0.481471	0.530598	0.469402

[a] Large enough value was used but it is not meaningful. [b] Relative phase content in terms of atoms.

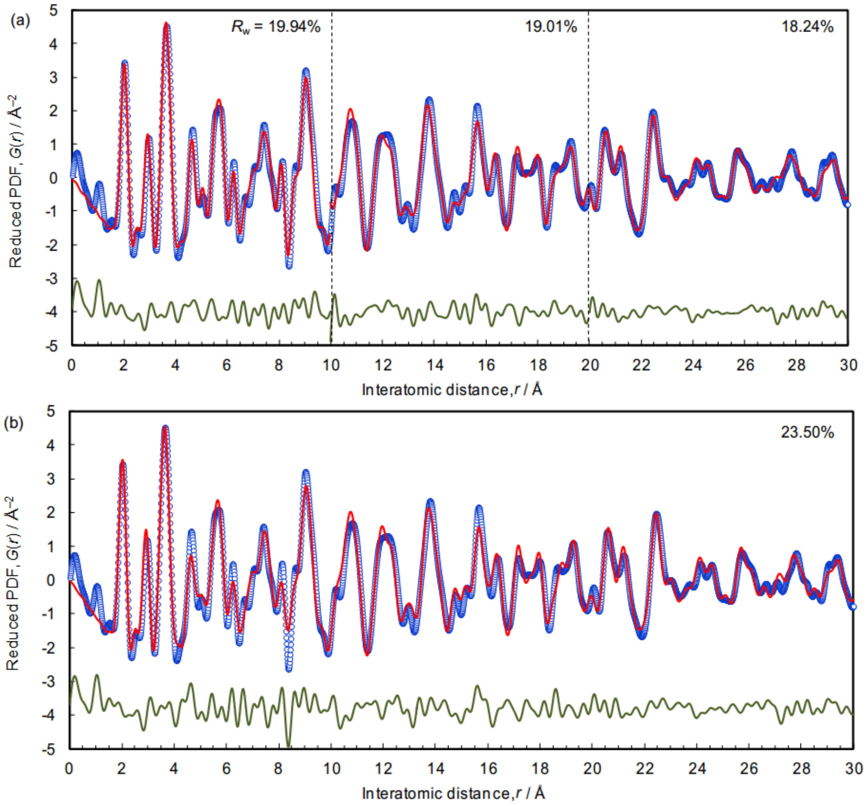

Fig. S14 PDF refinements of TiO_x-NP with a model based on Ti_2O_3 and Ti_4O_7. (a) Refinements at every 10 Å. (b) Refinement in the range from 0 to 30 Å. Experimental PDF plots (blue dots) with calculated ones based on corundum Ti_2O_3 (red line). Their difference is at the bottom (green curve).

Rutile TiO_2 nanoparticles reduced by CaH_2
Atomic structure analyzed by the PDF refinements in different *r* ranges (10 Å pitch)
3. Mixed phases of Ti_2O_3 and Ti_5O_9

Table S10 Atomic structure data of TiO_x-NP analyzed by PDF refinements (Ti_2O_3+Ti_5O_9).

Fitting range	0.01–10 Å		10–20 Å		20–30 Å		30–40 Å		0.01–30 Å	
R_w (%)	25.47		17.6408		17.248		34.1553		27.0113	
	Ti_2O_3 $R\bar{3}c$	Ti_5O_9 $P\bar{1}$	Ti_2O_3 $R\bar{3}c$	Ti_5O_9 $P\bar{1}$	Ti_2O_3 $R\bar{3}c$	Ti_5O_9 $P\bar{1}$	Ti_2O_3 $R\bar{3}c$	Ti_5O_9 $P\bar{1}$	Ti_2O_3 $R\bar{3}c$	Ti_5O_9 $P\bar{1}$
a / Å	5.09547 (3.4e-006)	5.36831 (1.6e-005)	5.10229 (2e-006)	5.41901 (1.1e-005)	5.08932 (1.8e-006)	5.48782 (1.3e-005)	5.09681 (4.2e-006)	5.41178 (2.2e-005)	5.09047 (7.9e-007)	5.47004 (4.1e-006)
b / Å	$= a$	7.20117 (1.8e-005)	$= a$	7.22065 (1.3e-005)	$= a$	7.20001 (1.3e-005)	$= a$	7.25401 (2.9e-005)	$= a$	7.3341 (5e-006)
c / Å	13.8546 (1.7e-005)	8.94069 (2.3e-005)	13.8285 (7.7e-006)	8.86 (1.2e-005)	13.7986 (9e-006)	8.86622 (1.1e-005)	13.7691 (1.3e-005)	8.93187 (3.9e-005)	13.7926 (4e-006)	8.88012 (7.6e-006)
α (°)	90	101.06 (0.00018)	90	99.793 (0.00011)	90	100.472 (0.00014)	90	100.974 (0.00032)	90	101.637 (6.2e-005)
β (°)	90	112.845 (0.00016)	90	111.906 (0.00014)	90	110.684 (0.00016)	90	110.496 (0.00036)	90	111.53 (5.2e-005)
γ (°)	120	105.035 (0.00022)	120	107.1 (0.00018)	120	108.442 (0.00023)	120	107.788 (0.00021)	120	108.107 (6e-005)
$U_{iso,Ti}$ / Å^2	0.00518022 (2.8e-007	0.00518022 (2.8e-007	0.00897196 (3.5e-007)	0.00897196 (3.5e-007)	0.0139736 (7.6e-007)	0.0139736 (7.6e-007)	0.0323806 (3.4e-006)	0.0323806 (3.4e-006)	0.0100485 (1.9e-007)	0.0100485 (1.9e-007)
$U_{iso,O}$ / Å^2	0.0187193 (9e-007)	0.0187193 (9e-007)	0.032252 (2.1e-006)	0.032252 (2.1e-006)	0.0197495 (2.6e-006)	0.0197495 (2.6e-006)	0.0295374 (6e-006)	0.0295374 (6e-006)	0.0152363 (5.4e-007)	0.0152363 (5.4e-007)
Particle diameter / Å	–[a]	–[a]	–[a]	–[a]	–[a]	–[a]	–[a]	–[a]	52.3854	321.133
Phase content [b]	0.577732	0.422268	0.668019	0.331981	0.74403	0.25597	0.874019	0.125981	0.684154	0.315846

[a] Large enough value was used but it is not meaningful. [b] Relative phase content in terms of atoms.

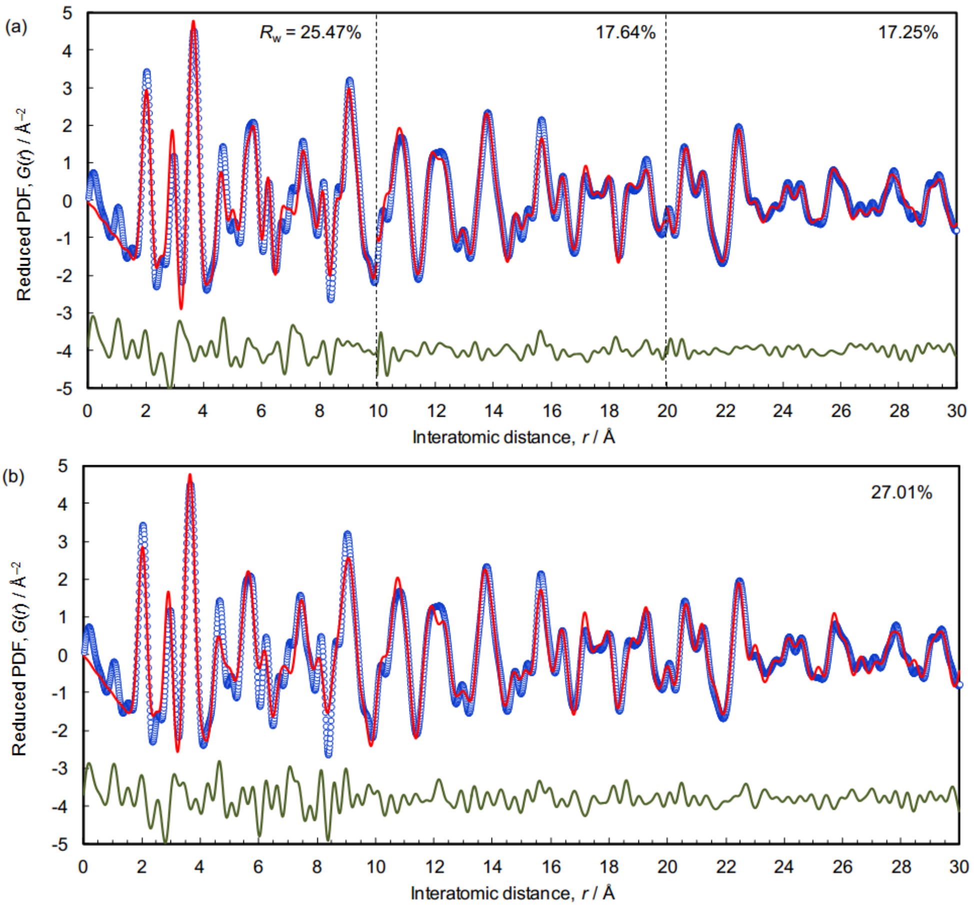

Fig. S15 PDF refinements of TiO_x-NP with a model based on Ti_2O_3 and Ti_5O_9. (a) Refinements at every 10 Å. (b) Refinement in the range from 0 to 30 Å. Experimental PDF plots (blue dots) with calculated ones based on corundum Ti_2O_3 (red line). Their difference is at the bottom (green curve).

Rutile TiO_2 nanoparticles reduced by CaH_2

Atomic structure analyzed by the PDF refinements in different *r* ranges (10 Å pitch)

4. Mixed phases of Ti_2O_3 and Ti_6O_{11}

Table S11 Atomic structure data of TiO_x-NP analyzed by PDF refinements (Ti_2O_3+Ti_6O_{11}).

Fitting range	0.01–10 Å		10–20 Å		20–30 Å		30–40 Å		0.01–30 Å	
R_w (%)	19.654		20.8037		21.2726		36.9974		24.3367	
	Ti_2O_3	Ti_6O_{11}	Ti_2O_3	Ti_6O_{11}	Ti_2O_3	Ti_6O_{11}	Ti_2O_3	Ti_6O_{11}	Ti_2O_3	Ti_6O_{11}
	$R\bar{3}c$	$I\bar{1}$	$R\bar{3}c$	$I\bar{1}$	$R\bar{3}c$	$I\bar{1}$	$R\bar{3}c$	$I\bar{1}$	$R\bar{3}c$	$I\bar{1}$
a / Å	5.08366	5.46154	5.10337	5.48502	5.08668	5.43378	5.09411	5.4559	5.08719	5.46333
	(2.4e-006)	(1.8e-005)	(1.8e-006)	(1.2e-005)	(1.9e-006)	(1.3e-005)	(4.1e-006)	(3.2e-005)	(7.5e-007)	(6.9e-006)
b / Å	= a	7.18497	= a	7.34093	= a	7.32638	= a	7.4226	= a	7.30065
		(1.8e-005)		(1.6e-005)		(1.7e-005)		(4.9e-005)		(7.4e-006)
c / Å	13.8431	32.1316	13.7793	31.2816	13.8082	32.0522	13.7688	31.7812	13.8231	31.992
	(1.7e-005)	(0.00017)	(1.1e-005)	(6.9e-005)	(1.1e-005)	(8.8e-005)	(1.8e-005)	(0.00013)	(4.1e-006)	(3.6e-005)
α (°)	90	65.9036	90	67.5806	90	66.6423	90	67.0794	90	67.109
		(0.00025)		(0.00021)		(0.00028)		(0.00062)		(0.00011)
β (°)	90	56.6565	90	57.6094	90	58.0146	90	57.9224	90	57.704
		(0.00024)		(0.00013)		(0.00016)		(0.00053)		(8.5e-005)
γ (°)	120	106.095	120	108.927	120	108.833	120	108.989	120	109.001
		(0.00028)		(0.00021)		(0.00026)		(0.0005)		(9.5e-005)
$U_{iso,Ti}$ / $Å^2$	0.0040007	0.00867751	0.010541	0.010541	0.0125195	0.0125195	0.0221519	0.0221519	0.00867751	0.00867751
	(1.6e-007)	(1.1e-007)	(2.2e-007)	(2.2e-007)	(5e-007)	(5e-007)	(1.5e-006)	(1.5e-006)	(1.1e-007)	(1.1e-007)
$U_{iso,O}$ / $Å^2$	0.0127748	0.014101	0.0098811	0.0098811	0.0154135	0.0154135	0.0180794	0.0180794	0.014101	0.014101
	(6.5e-007)	(4.4e-007)	(6.6e-007)	(6.6e-007)	(1.8e-006)	(1.8e-006)	(3e-006)	(3e-006)	(4.4e-007)	(4.4e-007)
Particle diameter / Å	–[a]	–[a]	–[a]	–[a]	–[a]	–[a]	–[a]	–[a]	48.4561	118.717
Phase content [b]	0.564708	0.435292	0.502637	0.497363	0.581336	0.418664	0.774804	0.225196	0.564708	0.435292

[a] Large enough value was used but it is not meaningful. [b] Relative phase content in terms of atoms.

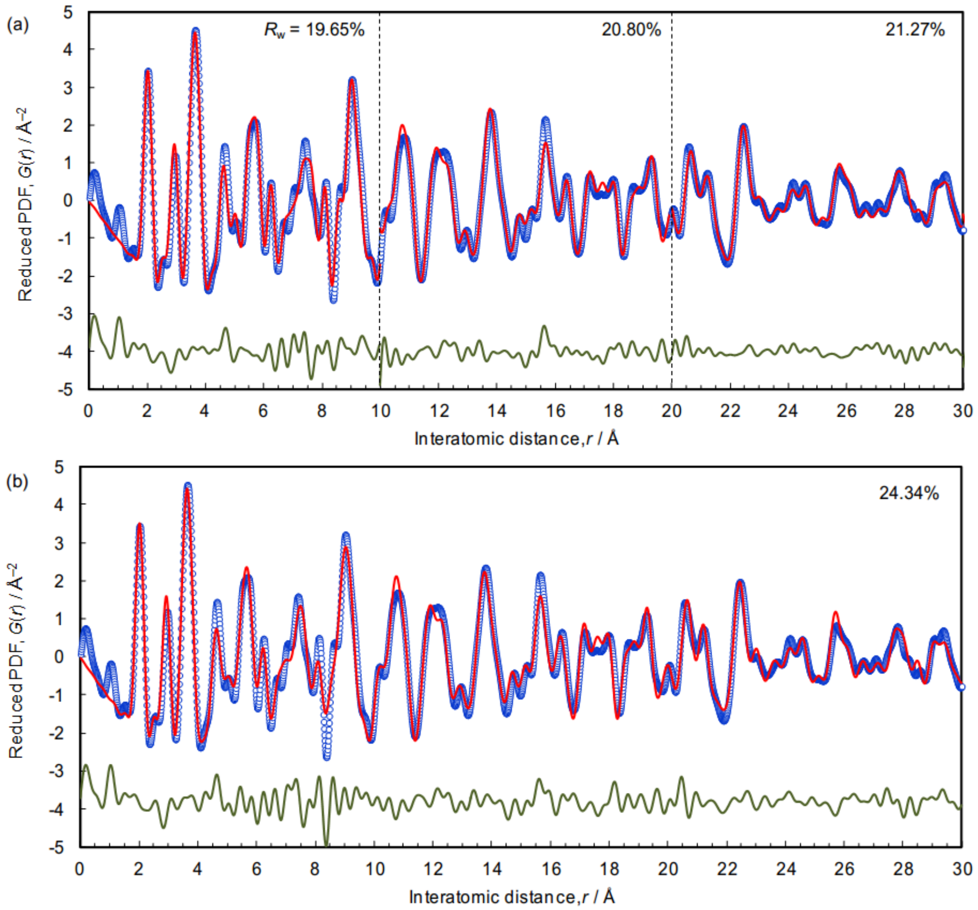

Fig. S16 PDF refinements of TiO_x-NP with a model based on Ti_2O_3 and Ti_6O_{11}. (a) Refinements at every 10 Å. (b) Refinement in the range from 0 to 30 Å. Experimental PDF plots (blue dots) with calculated ones based on corundum Ti_2O_3 (red line). Their difference is at the bottom (green curve).

Rutile TiO_2 nanoparticles reduced by CaH_2
Powder XRD patterns based on PDF refinement results

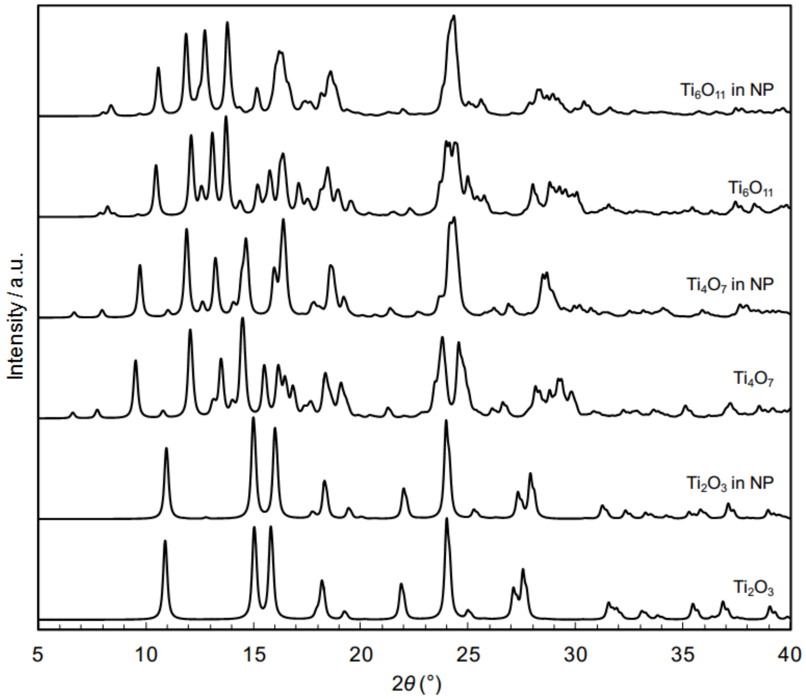

Fig. S17 Powder XRD patterns calculated from the crystal structures refined by the PDF method. **Ti_2O_3**: the corundum structure obtained from the commercially available Ti_2O_3. **Ti_2O_3-NP**: the corundum structure obtained from the TiO_2 nanoparticles reduced by CaH_2. **Ti_4O_7**: the Magneli phase Ti_4O_7 (ICSD no. 35121). **Ti_4O_7-NP**: the Magneli phase Ti_4O_7 obtained from the TiO_2 nanoparticles reduced by CaH_2. **Ti_6O_{11}**: the Magneli phase Ti_6O_{11} (ICSD no. 48131). **Ti_6O_{11}-NP**: the Magneli phase Ti_6O_{11} obtained from the TiO_2 nanoparticles reduced by CaH_2. FWHM of peak shape is set to be 0.2° in 2θ.

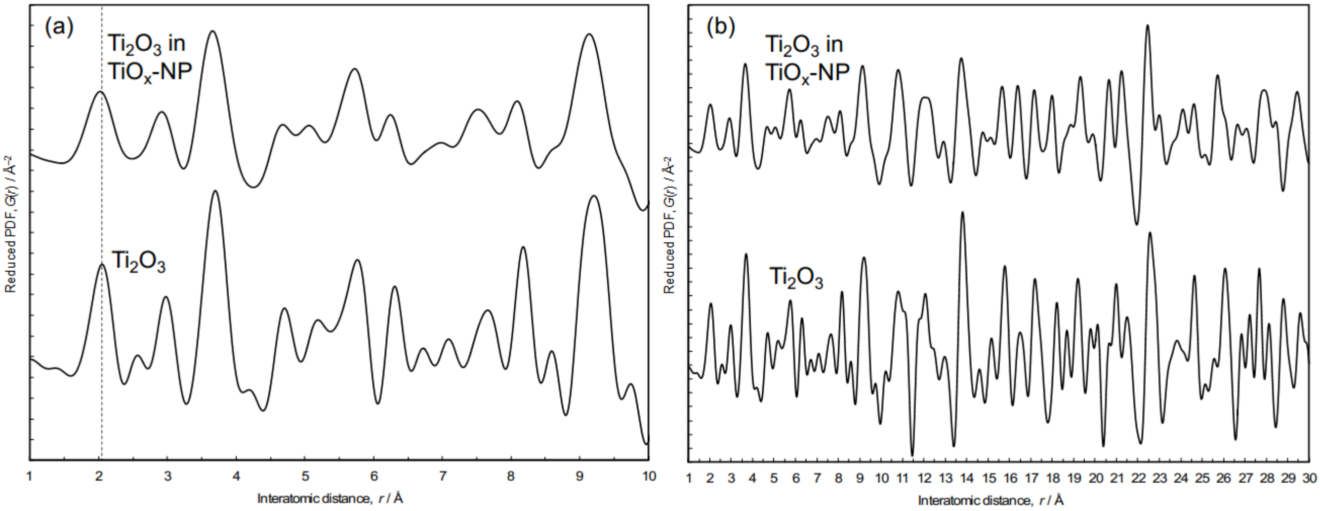

Fig. S18 PDFs calculated from crystal structures refined by the PDF method.

S6. Atomic structure of TiO_2 nanoparticles reduced by NaH_4

Table S12 Atomic structure data of TiO_2 nanoparticles reduced by $NaBH_4$ at 375°C analyzed by PDF refinements

Fitting range	0.01–10 Å		10–20 Å		20–30 Å		30–40 Å		0.01–30 Å	
R_w (%)	22.2455		22.441		29.014		41.6525		27.8073	
	Ti_2O_3	Ti_4O_7	Ti_2O_3	Ti_4O_7	Ti_2O_3	Ti_4O_7	Ti_2O_3	Ti_4O_7	Ti_2O_3	Ti_4O_7
	$R\bar{3}c$	$I\bar{1}$	$R\bar{3}c$	$I\bar{1}$	$R\bar{3}c$	$I\bar{1}$	$R\bar{3}c$	$I\bar{1}$	$R\bar{3}c$	$I\bar{1}$
a / Å	5.0459 (9.6e-006)	5.53704 (3.4e-005)	5.09307 (3.1e-006)	5.44896 (6.7e-006)	5.06235 (4.5e-006)	5.47261 (1.4e-005)	5.06253 (3.5e-006)	5.50474 (9.4e-006)	5.05816 (1.9e-006)	5.48301 (5.1e-006)
b / Å	$= a$	7.19729 (2.2e-005)	$= a$	7.44498 (1.1e-005)	$= a$	7.42805 (2e-005)	$= a$	7.41792 (1.1e-005)	$= a$	7.28713 (5.4e-006)
c / Å	14.0668 (5.9e-005)	20.698 (7.5e-005)	13.8363 (1.5e-005)	20.0907 (2.9e-005)	13.7486 (2.5e-005)	20.1399 (6.8e-005)	13.6499 (1.5e-005)	20.3002 (3.7e-005)	13.8919 (8.3e-006)	20.4355 (2.2e-005)
α (°)	90	67.156 (0.00045)	90	66.8745 (0.00013)	90	66.8459 (0.00028)	90	66.9489 (0.00012)	90	67.3395 (8.2e-005)
β (°)	90	57.1351 (0.00042)	90	57.8397 (0.00012)	90	57.9004 (0.00023)	90	57.5472 (0.00016)	90	57.1325 (7e-005)
γ (°)	120	108.543 (0.00028)	120	108.841 (0.00014)	120	108.777 (0.00028)	120	108.753 (0.00011)	120	108.597 (7.6e-005)
$U_{iso,Ti}$ / Å^2	0.00918728 (2.5e-007)	0.00918728 (2.5e-007)	0.0101075 (1.9e-007)	0.0101075 (1.9e-007)	0.0122871 (7.8e-007)	0.0122871 (7.8e-007)	0.0123018 (7e-007)	0.0123018 (7e-007)	0.0120645 (1.4e-007)	0.0120645 (1.4e-007)
$U_{iso,O}$ / Å^2	0.0127393 (9.5e-007)	0.0127393 (9.5e-007)	0.0185292 (1.2e-006)	0.0185292 (1.2e-006)	0.0124742 (1.7e-006)	0.0124742 (1.7e-006)	0.0177094 (1.9e-006)	0.0177094 (1.9e-006)	0.0110315 (3.8e-007)	0.0110315 (3.8e-007)
Phase content [b]	0.295899	0.704101	0.418987	0.581013	0.41647	0.58353	0.850953	0.149047	0.310909	0.689091

[b] Relative phase content in terms of atoms.

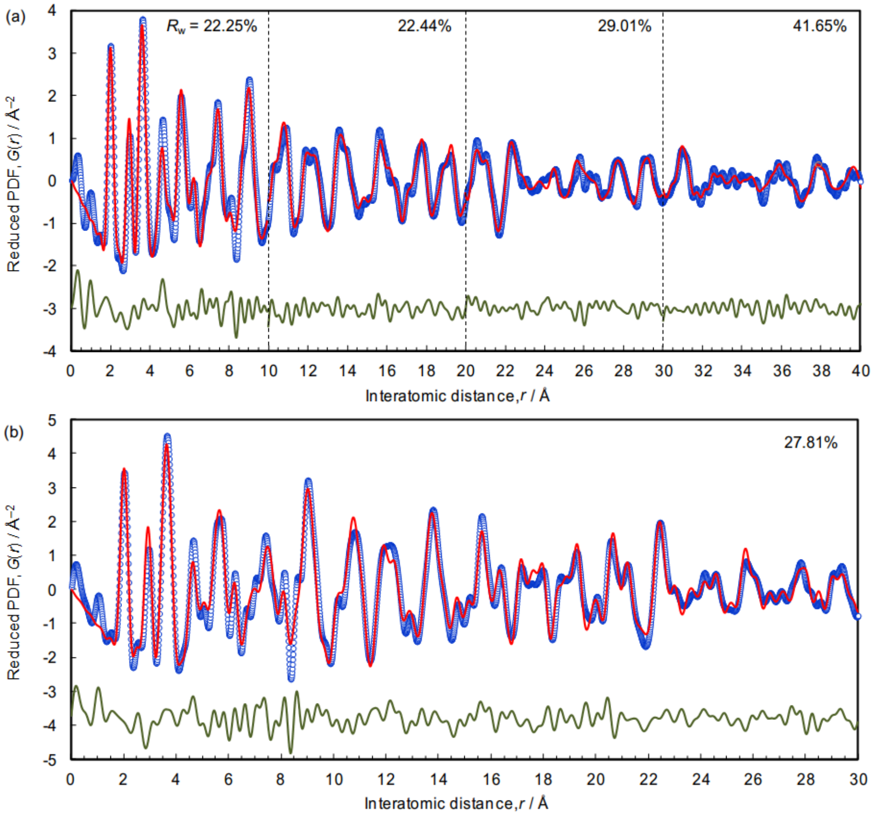

Fig. S19 PDF refinements of TiO_2 nanoparticles reduced using $NaBH_4$ at375°C with a model based on Ti_2O_3 and Ti_4O_7. (a) Refinements at every 10 Å. (b) Refinement in the range from 0 to 30 Å. Experimental PDF plots (blue dots) with calculated ones based on corundum Ti_2O_3 (red line). Their difference is at the bottom (green curve).

S7. Angle-resolved HX-PES of TiO_x-SC

Since the spectra collected at a low takeoff angle of 30° are identical to those at 88.5°, the influence of surface re-oxidization is negligible.

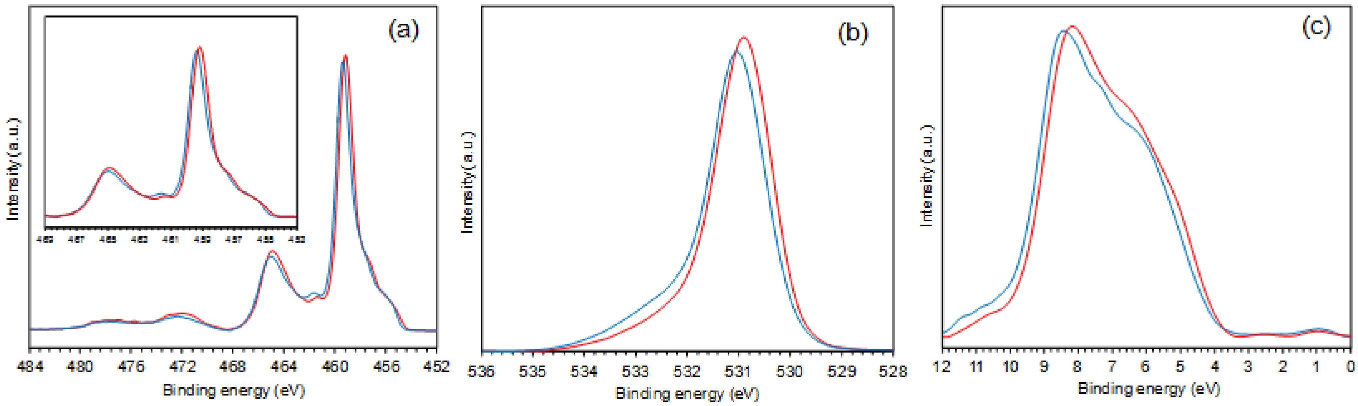

Fig. S20 Angle-resolved HX-PES of TiO_x-SC. The data were collected at a different takeoff angle of 88.5° (blue) and 30.0 (red): (a) Ti 2*p*, (b) O 1*s*, and (c) valence band.

S8. Discussion on impurities of TiO_x-SC

The influence of impurities such as OH species was considered to be negligible, judged from the faint peak around 13 eV attributable to those species.[12] The OH species were judged to be in a form of Ca(OH)_2 in view of the presence of negligible amount of Ca species. This confirmation is important for the following discussion, because OH species are one of the possible origins of the Ti^{3+} sites and might be generated by insertion of H atoms from the hydride.

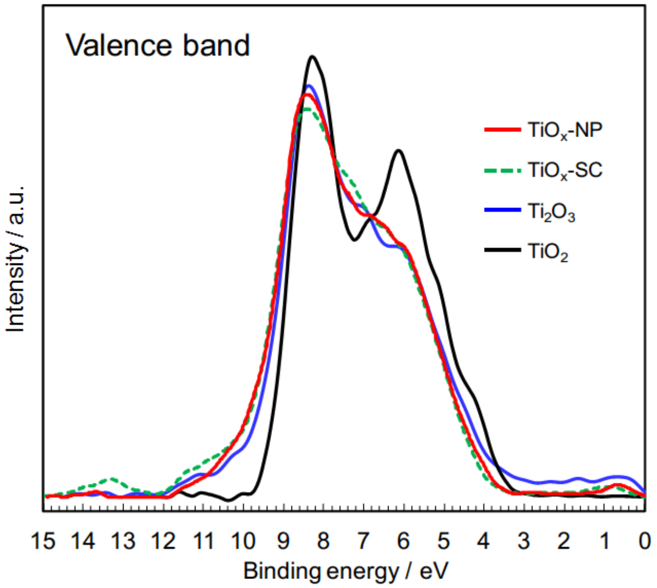

Fig. S21 HX-PES of the valence bands (takeoff angle of 88.5°).

S9. EELS without peak deconvolution

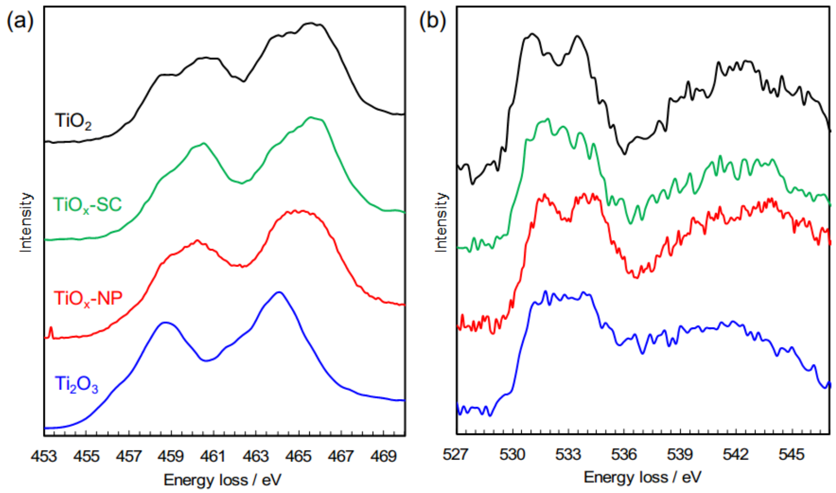

Fig. S22 Raw EELS with subtraction of background based on a power law. (a) Ti *L*-edge. (b) O *K*-edge.

S10. Optical absorption

TiO_x-SC and TiO_x-NP are black, but single crystalline Ti_2O_3 was reported to be purple.[13] The optical absorption spectra of TiO_x-SC (Fig. d) and TiO_x-NP (Fig. b) are similar to that of Ti_2O_3: The absorption above 3.5 eV is assignable to the transition from the valence band to the conduction band. The small peak around 3.0 eV is assignable to a transition from a_{1g} band to $e_g^{\sigma *}$ band. The leftmost peak around 1.4 eV is assignable to the transition from a_{1g} band to its a_{1g}* band, which is considered to be located between e_g^{π} and $e_g^{\sigma *}$. This a_{1g}-a_{1g}^* transition was reported to be <1.2 eV, but that of TiO_x-SC and TiO_x-NP is 1.4 eV. This shift is not consistent with the prediction from structure analyses. The spectrum of Ti_2O_3 particle is far different from the reported Ti_2O_3 spectrum, probably due to influence of specular reflectance. This did not get better even by manual grinding using a pestle and mortar.

The e_g^{π} band is considered to be located just above the Fermi level, because the valence band maximum energies (Fig. 2b, inset) are the same as the optical bandgap of ~3.5 eV. More precisely, from O 1s HX-PES peaks (531.07 eV for TiO_x-SC, 530.94 eV for TiO_x-NP and 531.02 eV for Ti_2O_3 in Fig. 2b) and O *K*-edge EELS peaks (531.30 eV, 531.35, 531.35 eV in Fig. 2d), the e_g^{π} band peaks in TiO_x-SC, TiO_x-NP and Ti_2O_3 are estimated to be at ~0.27, ~0.41 and ~0.33 eV above E_F.

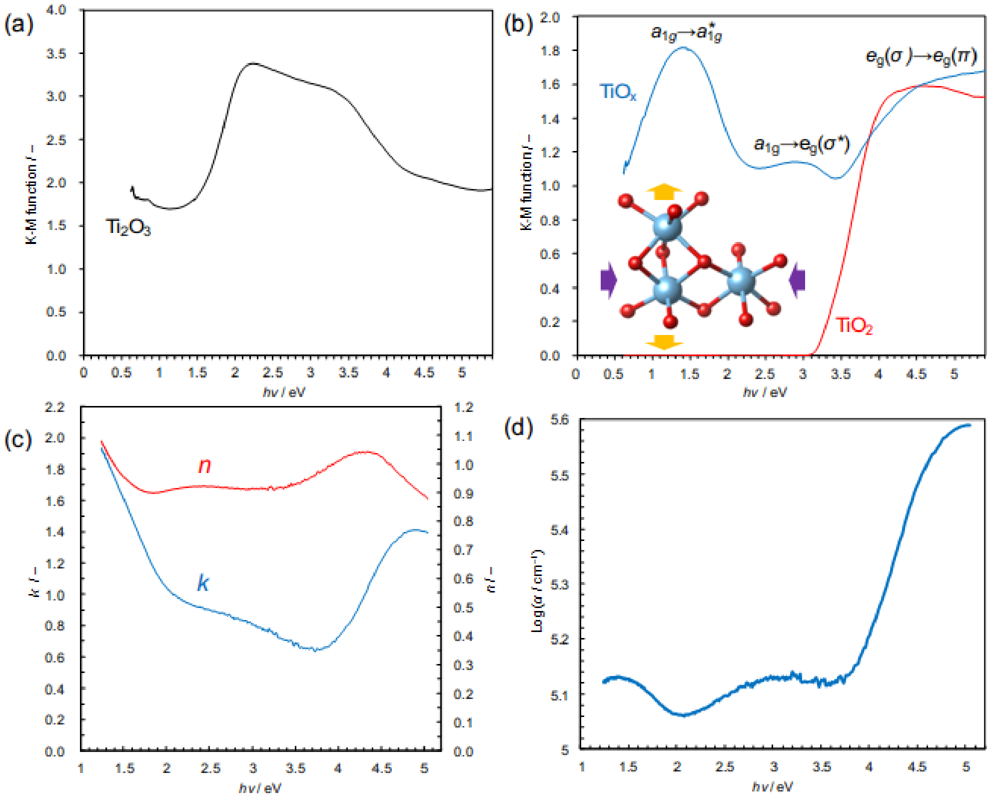

Fig. S23 Optical absorption spectra. (a, b) Kubelka–Munk (K–M) functions of powder samples: Ti_2O_3, TiO_2 and TiO_x-NP. The K–M functions were calculated from UV-vis-NIR spectra measured in the diffuse reflectance mode. (c) Optical constants, extinction coefficient *k* and refractive index *n*, of TiO_x-SC.

S11. Thermogravimetric analyses

The weight loss below ~120°C was assigned to the removal of solvent adsorbed on the surface, and thus the weight was normalized for the dried state. The compositions of TiO_x-NP and Ti_2O_3 are $TiO_{1.83}$ and $TiO_{1.53}$.

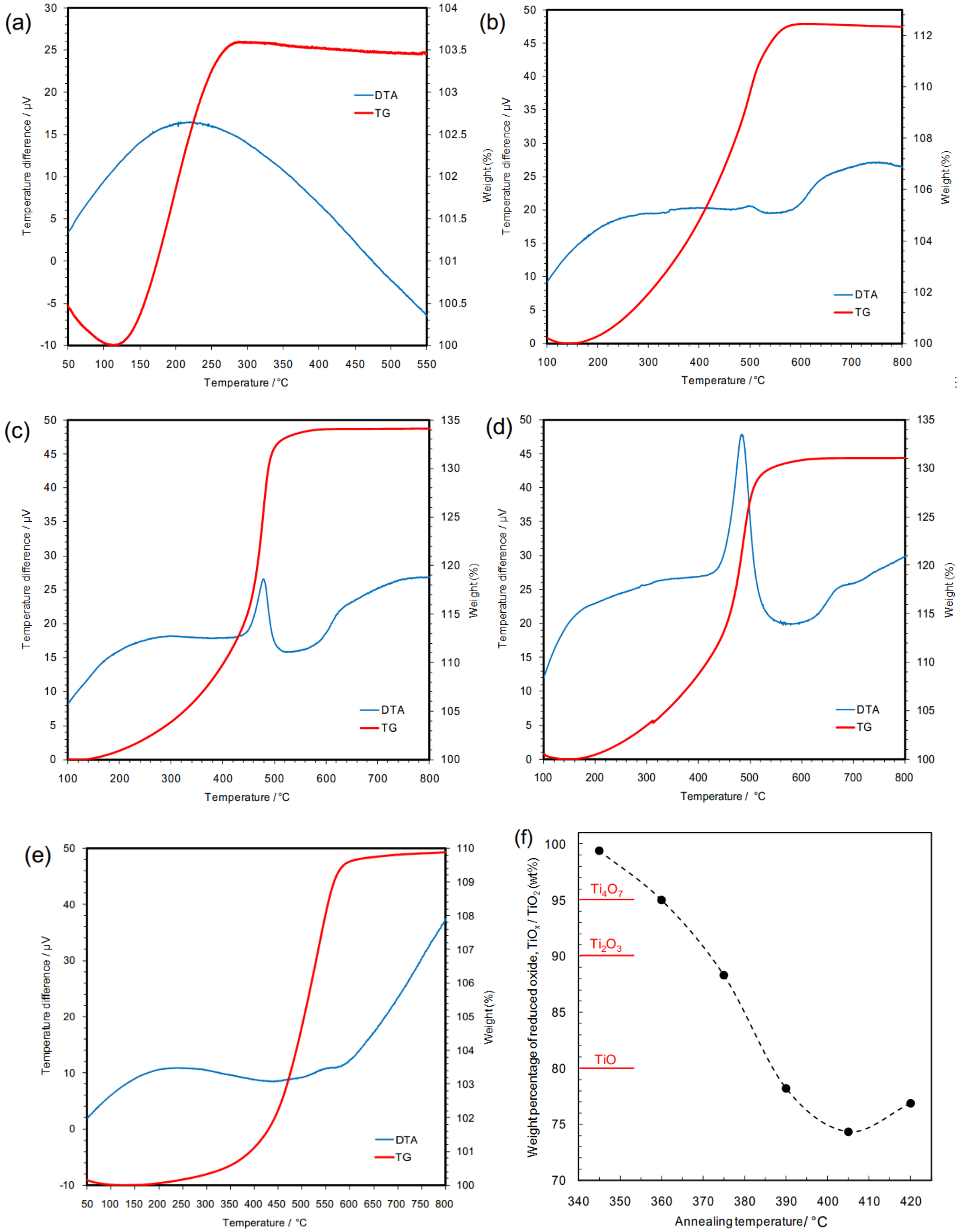

Fig. S24 Thermogravimetric analysis in air: (a) TiO_x-NP. (b) TiO_2 nanorods reduced by $NaBH_4$ at 375°C, (c) 405°C and (d) 420°C. (e) Ti_2O_3. (f) Compositions of TiO_2 nanorods reduced by $NaBH_4$ at a different temperature, on the assumption that the weight increase results from oxidation of TiO_x.

S12. Conductivity measurements "TiO$_x$-SC"

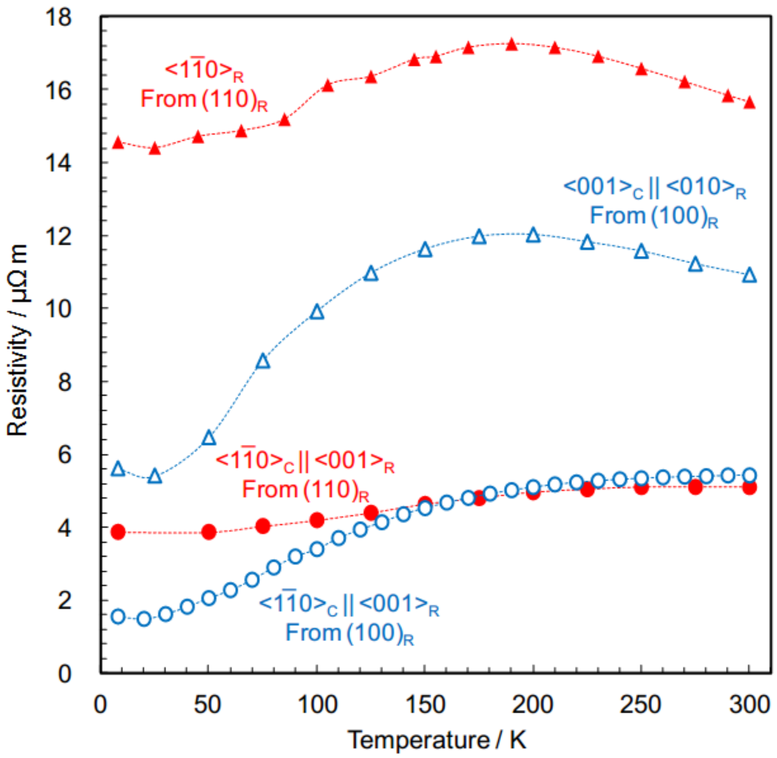

Fig. S25 Temperature dependence of electronic resistance measured along two different crystallographic directions. (**Blue**) (100)-oriented rutile TiO_2 single crystals reduced by CaH_2. (Circle) Along the <001>$_R$ of rutile, which equals to the <1$\bar{1}$0>$_C$ direction of the corundum phase of the reduced phase. (Triangle) Along the <010>$_R$ direction of rutile, which equals to the <001>$_C$ direction of the corundum phase of the reduced phase. (**Red**) (110)-oriented rutile TiO_2 single crystals reduced by CaH_2. (Circle) Along the <001>$_R$ of rutile, which equals to the <1$\bar{1}$0>$_C$ direction of the corundum phase of the reduced phase. (Triangle) Along the <1$\bar{1}$0>$_R$ direction of rutile.

References

1. S. Tominaka, Y. Tsujimoto, Y. Matsushita and K. Yamaura, *Angew. Chem. Int. Edit.*, 2011, **50**, 7418-7421.
2. S. Tominaka, *Inorg. Chem.*, 2012, **51**, 10136-10140.
3. S. Tominaka, *Chem. Commun.*, 2012, **48**, 7949-7951.
4. X. Qiu, J. W. Thompson and S. J. L. Billinge, *J. Appl. Cryst.* , 2004, **37**, 678-678.
5. C. L. Farrow, P. Juhas, J. W. Liu, D. Bryndin, E. S. Bozin, J. Bloch, T. Proffen and S. J. L. Billinge, *Journal of Physics-Condensed Matter*, 2007, **19**, art. no. 335219.
6. R. C. Howell, T. Proffen and S. D. Conradson, *Physical Review B*, 2006, **73**, art. no. 094107.
7. A. C. Larson and R. B. V. Dreele, *Los Alamos National Laboratory Report LAUR*, 2000, 86-748.
8. B. H. Toby, *J. Appl. Cryst.* , 2001, **34**, 210-213.
9. M. P. Seah and W. A. Dench, *Surf. Interface Anal.*, 1979, **1**, 2–11.
10. J. Verbeeck and S. Van Aert, *Ultramicroscopy*, 2004, **101**, 207-224.
11. L. A. Grunes, R. D. Leapman, C. N. Wilker, R. Hoffmann and A. B. Kunz, *Phys. Rev. B*, 1982, **25**, 7157-7173.
12. S. Krischok, O. Hofft, J. Gunster, J. Stultz, D. W. Goodman and V. Kempter, *Surf. Sci.*, 2001, **495**, 8-18.
13. S. S. M. Lu, F. H. Pollak and P. M. Raccah, *Phys. Rev. B*, 1978, **17**, 1970-1975.